CHARACTERIZING ROX: A RIFAMYCIN MONOOXYGENASE

CHARACTERIZING THE MECHANISM AND REGULATION OF A RIFAMYCIN MONOOXYGENASE IN *STREPTOMYCES VENEZUELAE*

By JAYNE KELSO, B.Sc.

A Thesis Submitted to the School of Graduate Studies in Partial Fulfillment of the Requirements for the Degree Master of Science

DESCRIPTIVE NOTE

McMaster University

Department of Biochemistry and Biomedical Science

Hamilton, Ontario, Canada

MASTER OF SCIENCE (2016)

TITLE: Characterizing the mechanism and regulation of a rifamycin monooxygenase in *Streptomyces venezuelae*

AUTHOR: Jayne Kelso, B.Sc. (McMaster University)

SUPERVISOR: Dr. Gerard D. Wright

NUMBER OF PAGES: xiii, 86

Lay Abstract

Antibiotic resistance represents a major threat to global health. Infections that were once readily treatable are no longer so due to the rise in multidrug resistant bacteria. As our arsenal of effective antibiotics is depleted, new drugs are being discovered less and less frequently. This has caused the scientific community to get creative in coming up with treatments: trying combinations of antibiotics, using antibiotics which were once considered too toxic, and repurposing antibiotics for different bacteria.

Rifamycins are a class of antibiotics most commonly used in the treatment of tuberculosis. However, they are becoming more widely used as a result of antibiotic resistance. There are a number of different ways bacteria can become resistant to the harmful effects of rifamycins: by modifying the target so the drug can no longer bind to it, actively pumping the drug out of the cell, or by changing the drug in some way so it is no longer effective. Bacteria in the environment use antibiotics as a form of chemical warfare to gain an advantage over their neighbours; therefore, they have had millions of years to evolve very effective methods of antibiotic resistance. By surveying what kinds of antibiotic resistance are in the environment, we can predict what we might see one day in a medical setting.

In this thesis, I have studied a protein that bacteria make to inactivate rifamycins. The rifamycin monooxygenase Rox adds an oxygen to the rifamycin scaffold; this causes spontaneous cleavage of the rifamycin backbone and changes the conformation of the drug so it can no longer bind to its target. I have also investigated the regulation of this and other genes in the bacterial strain *Streptomyces venezuelae.* By understanding how

this process works, we can potentially design inhibitors to stop this from happening, should this method of resistance ever become clinically prevalent.

Abstract

The rifamycins are a class of antibiotics which were once used almost exclusively to treat tuberculosis, but are currently receiving renewed interest. Resistance to rifamycins is most commonly attributed to mutations in the drug target, RNA polymerase. Yet environmental isolates are also able to enzymatically inactivate rifamycins in a number of ways. Recently, rifamycin resistance determinants from the environment were found to be closely associated with a so called rifamycin associated element (RAE). The region containing the RAE from an environmental strain was shown to induce gene expression in the presence of rifamycins, hinting at an inducible system for rifamycin resistance. In this work, we examine the RAE from a model organism for *Streptomyces* genetics, *Streptomyces venezuelae*. We confirm that the promoter region containing the RAE upstream of a rifamycin monooxygenase *rox* is inducible by rifamycins. The strains of *S. venezuelae* generated in this work can be used in future genetic studies on the RAE.

As well, the rifamycin monooxygenase Rox was purified for the first time and characterized biochemically. The structure of Rox was obtained with and without the substrate rifampin. Steady state kinetics for the enzyme were determined with a number of substrates, and its ability to confer resistance to rifamycins was examined. Monooxygenated rifamycin SV compound was purified and structurally characterized by NMR analysis. We proposed an aromatic hydroxylase type mechanism for Rox, in which the enzyme hydroxylates the aromatic core of the rifamycin scaffold and causes a non-enzymatic C-N bond cleavage of the macrolactam ring. This is a new mechanism of

rifamycin resistance, and sheds some light on the decomposition of rifamycins mediated by monooxygenation, which is still poorly understood.

Acknowledgments

My time as a graduate student at McMaster has been full of personal challenges, both educational and emotional. I first and foremost need to thank my supervisor Dr. Gerry Wright, who tried his best to teach me that there is no crying in science. Thank you for taking a chance on me and bringing me into the absolute best environment to do science. Your vast knowledge and dedication to your trainees will never be forgotten. I cannot thank you enough for all the experiences and opportunities you gave me. Thanks also to my committee members, Dr. Marie Elliot and Dr. Lori Burrows. Your kindness and support made me feel calm and capable when I needed it.

I have had the pleasure of working with some of the most talented minds while in the Wright lab. My work would not have been possible without the collaborative atmosphere of the lab. Special thanks to Dr. Kalinka Koteva for taking me under her wing when I arrived. You were instrumental in this project from day one, and I could not have done it without you. Whether I needed help generating and analyzing data, or just someone to hug, you were always there. Thank you also to Dr. Georgina Cox who was a fantastic mentor to a young scientist, and without whom the crystal structure would not have been possible.

To everyone else in the Wright lab who I had the pleasure of seeing every day, thank you for making me feel so at home. I will never forget all of our wonderful memories: winning the spirit award, countless games of Bang, lab retreats, decorating at Christmas, birthday cakes, Disney princesses, high tea, and so many more. I am so lucky to have met some wonderful grad students who kept me sane and somehow never tired of me. Beth, Arthur, and Matt, thanks for your friendship and your continuing positivity when my science got me down. To Austin Yan who at the beginning felt like my only friend, thank you for adopting me as a roommate and helping me get my feet on the ground in #thisgreatcity. And to Rachel Fong, who spent countless nights with me in lab even though she surely had better things to do, I am so lucky that you have become one of my dearest friends.

I have loved living in Hamilton for these past two years. Thank you to Philpott Memorial Church for welcoming me with open arms, and to Ronald McDonald House for letting me give back. I grew into the person I want to be here, and this city will always feel like home.

Lastly, I need to thank my sister Susan, who as always is my sounding board, in science and in life. And my parents Tom and Jeannie for your continued love and support, even when you had no idea what I was talking about. Thanks for taking care of me through all the madness.

Table of Contents

List of Figures

Chapter 1. Introduction

Chapter 2. Characterizing the RAE in *Streptomyces venezuelae*

Chapter 3. Characterizing the rifamycin monooxygenase Rox

List of Tables

List of Abbreviations

1D	One dimensional
2D	Two dimensional
ADP	Adenosine diphosphate
AHBA	3-amino-5-hydroxybenzoic acid
AMP	Adenine monophosphate
ART	ADP ribosyl transferase
ATP	Adenine triphosphate
BIS TRIS	2- [Bis (2-hydroxyethyl) amino]-2-(hydroxymethyl) propane-1,3-diol
blastn	Basic local alignment search tool- nucleotide
CLSI	Clinical and Laboratory Standards Institute
DMSO	Dimethyl sulfoxide
DNA	Deoxyribonucleic acid
DNase	Deoxyribonuclease
FAD	Flavin adenine dinucleotide
FADH2	Flavin adenine dinucleotide reduced
FMO	Flavin monooxygenase
FPLC	Fast protein liquid chromatography
GT	Glycosyltransferase
HEPES	4-(2-hydroxyethyl)-1-piperazineethanesulfonic acid
HPLC	High performance liquid chromatography
HSQC-15N	15N heteronuclear single-bond correlation
IPTG	Isopropyl β-D-1thiogalactopyranoside
LB	Lysogeny broth
LC/MS	Liquid chromatography mass spectrometry
MAD	Multiple wavelength anomalous diffraction
MES	2- (N-morpholino) ethanesulfonic acid
MIC	Minimum inhibitory concentration
mRNA	Messenger ribonucleic acid
NAD+	Nicotinamide adenine dinucleotide
NADB	NAD binding
NADH	Nicotinamide adenine dinucleotide reduced
NADP+	Nicotinamide adenine dinucleotide phosphate
NADPH	Nicotinamide adenine dinucleotide phosphate reduced
Ni-NTA	Nickel-nitrilotriacetic acid
NMR	Nuclear magnetic resonance
ORF	Open reading frame
PCR	Polymerase chain reaction
PDB	Protein database
PEG	Polyethylene glycol
PEGm	Poly (ethylene glycol) methyl ether
PEP	Phosphoenol pyruvate

pHBH	para-hydroxybenzoate hydroxylase
PPSA	Phosphoenol pyruvate synthase
RAE	Rifamycin associated element
RIFAB	Rifabutin
RIFAP	Rifapentine
RIFAX	Rifaximin
RIF-B	Rifamycin B
RIF-O	Monooxygenated rifampin
RIF-S	Rifamycin S
RIF-SV	Rifamycin SV
RIF-SV-18O	RIF-SV-O labelled with 18O
RIF-SV-O	Monooxygenated rifamycin SV
RNA	Ribonucleic acid
RRDR	Rifamycin resistance determining region
SDS-PAGE	Sodium dodecylsulfate- polyacrylamide gel electrophoresis
SIM	*Streptomyces* isolation medium
TEV	Tobacco etch virus
TMS	Tetramethylsilane
UV-Vis	Ultraviolet-visible
WAC	Wright Actinomycete Collection
X-Gluc	5-bromo-4-chloro-3-indolyl b-D-glucuronide

DECLARATION OF ACADEMIC ACHEIVEMENT

Jayne Kelso performed the majority of experiments, data collection, and analysis presented here. The report was also written by Jayne.

Supervisor Dr. Gerry Wright, committee members Dr. Marie Elliot and Dr. Lori Burrows, and collaborators Dr. Kalinka Koteva and Dr. Georgina Cox provided guidance and direction during the project. As well, other members of the Wright lab assisted in troubleshooting and provided advice at times.

Transfer of Rox crystals to the X-ray diffraction system, X-ray diffraction data acquisition, and generation of the Rox crystal structure from the data was performed by Dr. Georgina Cox. Preparation of crystals by hanging drop vapor diffusion was performed by Jayne. All subsequent images and analysis of the Rox crystal structure was performed by Jayne.

Dr. Kalinka Koteva submitted the RIF-SV, RIF-S, and RIF-SV-O samples for NMR experiments, assigned all chemical shifts, and derived the structure. Jayne prepared the sample and compared the shifts between compounds.

Samples were run on the high resolution mass spectrometer by Dr. Koteva. Samples for mass spectrometry analysis were prepared by Jayne.

Chapter 1. Introduction

1.1 Antibiotics and resistance

Antibiotics have revolutionized modern medicine. The golden age of antibiotic discovery in 1940-1960 resulted in the development of many promising drugs that were predicted to eradicate infectious disease. However, the emergence of antibiotic resistance has never been far behind the discovery of a new compound. Fewer new antibiotics are developed each decade, while antibiotic resistant bacteria are on the rise. This "antibiotic paradox" has led to the current resistance crisis. Multidrug resistant bacteria represent one of the most serious threats to public health.

Many of our clinically used antibiotics are natural products or derivatives of natural product scaffolds produced by microorganisms. Antibiotics offer a competitive advantage in the environment and consequently antibiotic resistance is also widespread in the environment. Resistance determinants from the environment and the clinic are very similar, hinting that like antibiotics, resistance originates from the environment (1).

Bacteria employ a number of different strategies to overcome the effect of antibiotics. The entire collection of genes conferring resistance to antibiotics is termed the antibiotic resistome (2). It is important that we study both clinical and environmental determinants that comprise the resistome to adequately monitor the mutation and mobilization of potential resistance genes.

1.2 Rifamycin antibiotics

The rifamycins are an intriguing and invaluable class of antibiotics. They are part of the ansamycin family, characterized as having an aromatic core often derived from 3-amino-5-hydroxybenzoic acid (AHBA), and bridged on either side of this core by an aliphatic chain (3) (Figure 1.1). The rifamycins have a broad spectrum of activity and exquisite specificity for prokaryotes. Rifampin, the most widely used of the rifamycin antibiotics, has remained instrumental in the treatment of tuberculosis since its discovery 50 years ago.

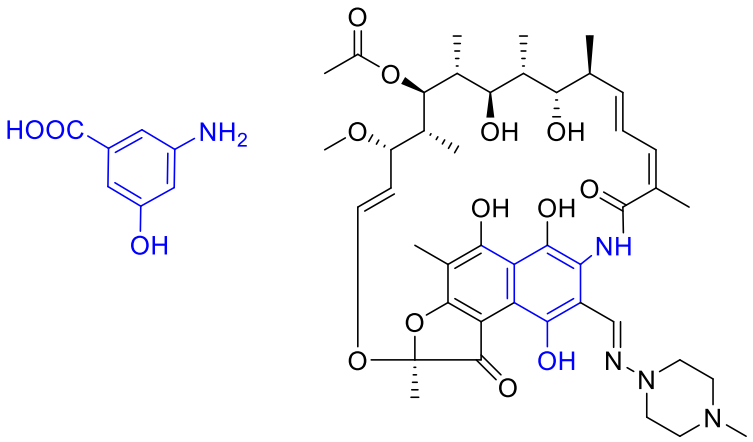

Figure 1.1 Structure of the AHBA core, and its position in rifampin.

1.2.1 Discovery of natural product rifamycins

In 1957, a mixture of compounds from *Streptomyces mediterranei* was found to have antibacterial activity (4). The individual components of this mixture were given names rifamycins A through E. All components were unstable and difficult to purify save for rifamycin B (RIF-B). RIF-B has no antibacterial activity per se; however, it is readily converted to rifamycin S (RIF-S) in aqueous solution, which is what seems to give RIF-B its activity. RIF-S can be reduced easily to rifamycin SV (RIF-SV) (4) (Figure 1.2). RIF-SV is highly active

towards Gram-positive bacteria, including *Mycobacterium tuberculosis*, and moderately active against Gram-negatives. However, it was poorly absorbed when taken orally, and when given parenterally it is quickly excreted by the liver (4). Nevertheless RIF-SV sodium salt was introduced as a topical and parenteral agent for Gram-positive infections and infections of biliary tract in 1963 (4).

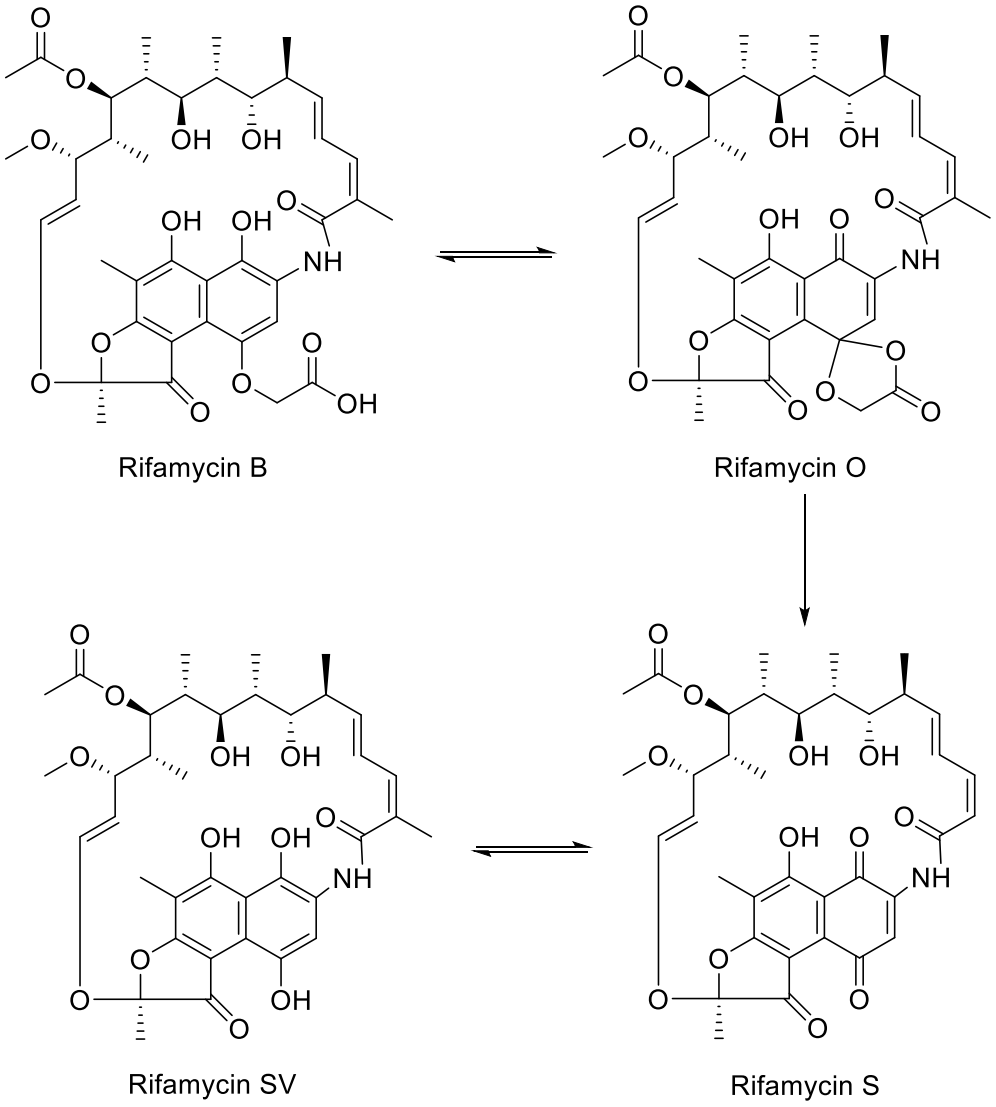

Figure 1.2 Natural conversion of RIF-B to RIF-SV in aqueous reducing environments. Figure adapted from (4).

1.2.2 Rifamycin structure activity relationships

Due to the pharmacological drawbacks of RIF-SV, an effort was undertaken to create better rifamycin antibiotics. Extensive chemical modification of RIF-SV uncovered some important structure activity relationships. Modifications resulting in a conformational change in the ansa chain diminished activity (4) (Figure 1.2). The hydroxyl residues at C21, C23 and C8 were also essential. An oxygen group on C1 was necessary for activity, though it did not matter if it was a ketone or a hydroxyl moiety. Modifications to C3 and C4 were tolerated quite well. The low level of activity of RIF-B was attributed to poor penetration through the cell wall due to the carboxyl group on C4. This information was key to rational design of better rifamycin antibiotics.

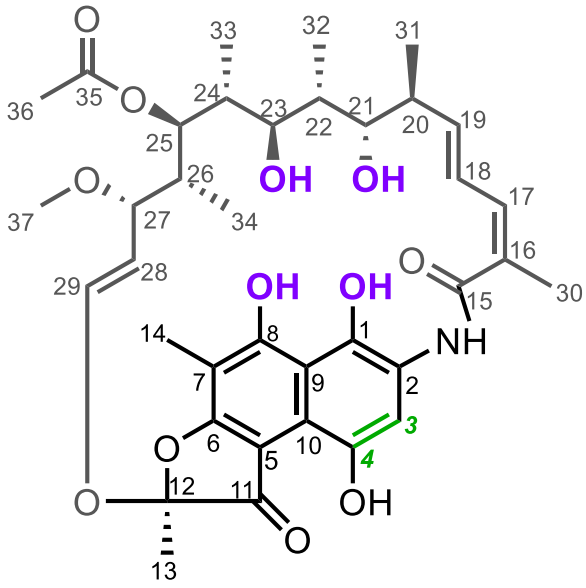

Figure 1.3 Structure of natural product RIF-SV. The various features identified by SAR studies are highlighted. The ansa- chain is coloured gray; conformational changes to this region negatively affects activity. The four key hydroxyl groups are highlighted in purple. Carbons 3 and 4 are amenable to semisynthetic modification, and are highlighted in green.

1.2.3 Medicinal chemistry and derivatization

Guided by the structure activity relationships, derivatization at the C3 and C4 position yielded a wide variety of compounds. By adding different chemical groups at these positions, properties like absorption from the gastrointestinal tract, excretion, and uptake by bacterial cells could be manipulated (4). Amide derivatives of RIF-SV were investigated for their pharmacokinetic properties and had marginally better efficacy. The best candidate of these, rifamide, was introduced as a drug in 1965, but overall was not much better than RIF-SV (4). Continued semi-synthesis generated a particularly effective compound, which researchers called rifampin. Rifampin has a hydrazone linked piperazine ring at the C3 position (Figure 1.4). The addition of this group significantly improved the activity and stability of the drug, and rifampin has since become a frontline agent in the treatment of tuberculosis (4). However, rifampin still had a few drawbacks, including toxicity issues and a high frequency of resistance (5). Thus semi-synthesis continued in efforts to create a drug without these drawbacks. Rifapentine (RIFAP) was approved for use in 1998 and had a longer half life than rifampin, only needing to be taken orally twice a week (5). Rifabutin (RIFAB) was approved in 1992 for the treatment of the *Mycobacterium avium* complex in AIDS patients (5). The latest rifamycin approved for clinical use is Rifaximin (RIFAX), which was approved in 2004 for the treatment of *Escherichia coli* causing travellers diarrhea (5). The well defined structure activity relationships make the rifamycin scaffold an attractive canvas for continued derivatization.

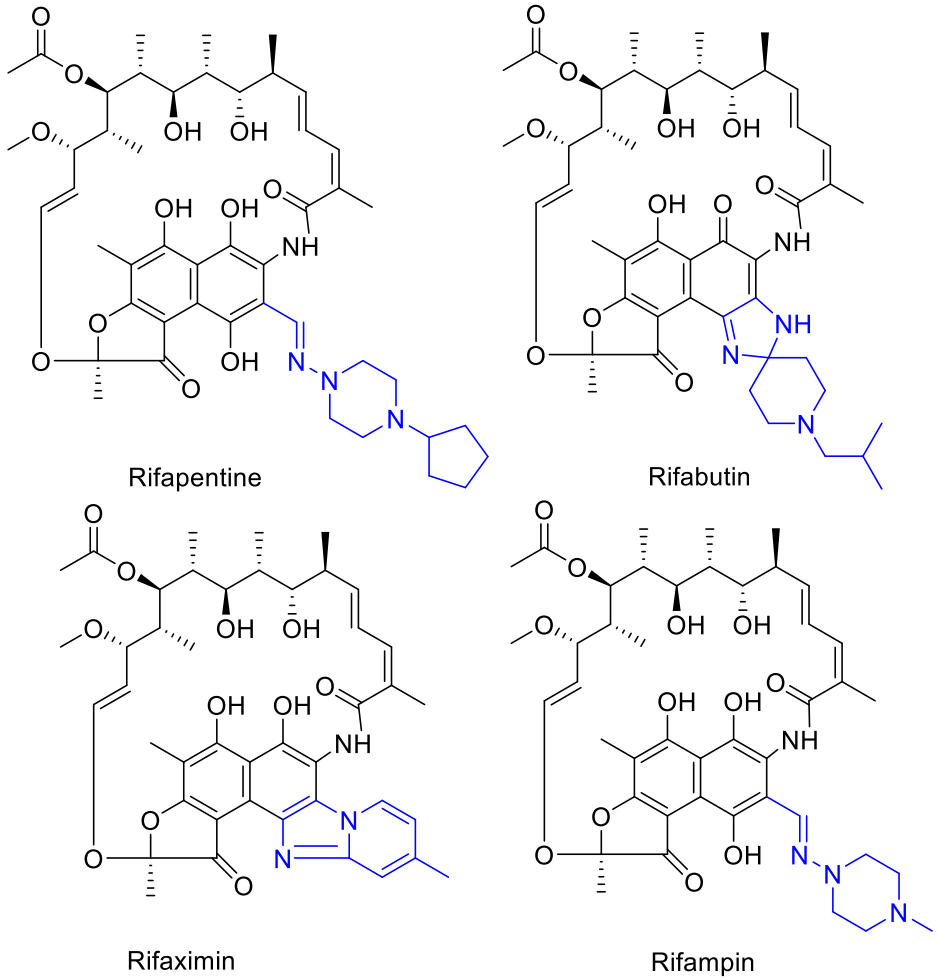

Figure 1.4 Semisynthetic rifamycin derivatives. The synthetic part of the molecule is highlighted in blue

1.2.4 Mechanism of action

Rifamycins are inhibitors of bacterial RNA synthesis, which represented a new drug target at the time of their discovery (6–8). In 1968, Wehrli and coworkers showed that rifamycins bind to RNA polymerase, and McClure and Cech showed that *in vitro* transcription in the presence of rifamycins resulted in the accumulation of short chains of 2-3 nucleotides (8,9). Taken together, these results suggested a steric occlusion model in which rifamycins physically block the transcription of mRNA. When Campbell and coworkers crystalized RNA polymerase

in complex with rifampin in 2001, this was found to be exactly the case (10). Key interactions between the rifamycin scaffold and the beta subunit of RNA polymerase (RpoB) depend on the hydroxyl residues at positions C1, C8, C21 and C23 (Figure 1) (10). This explains the importance of these moieties in the structure activity relationship studies. As well, the conformation of the rifamycin molecule is critical for the drug to interact with the target, explaining the necessity of an unmodified ansa chain. A number of amino acids in RpoB are also involved in hydrophobic interactions with the aromatic core of the rifamycin scaffold. Importantly, the semisynthetic tail region of rifampin does not make any interactions with the enzyme (Figure 1.5).

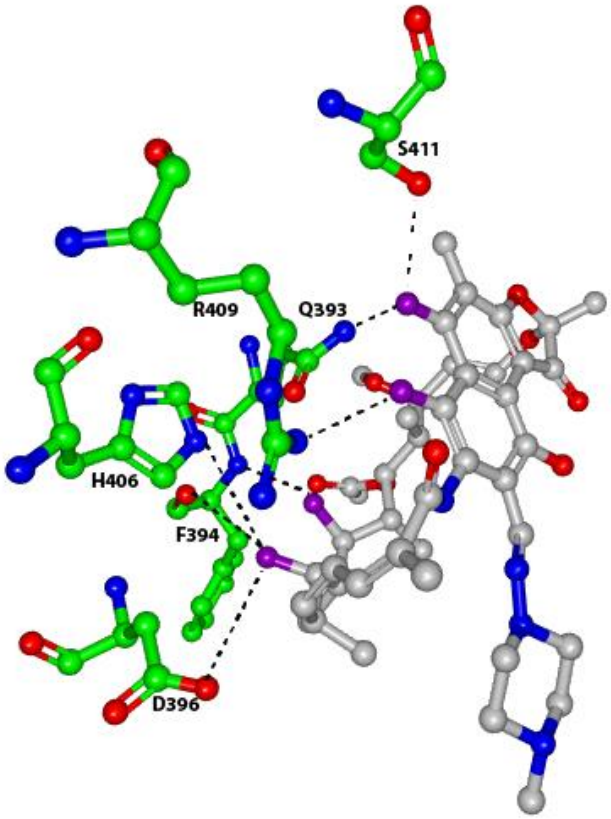

Figure 1.5 Crystal structure of rifampin bound to RNA polymerase. Residues of RpoB forming hydrogen bonds with RIF are shown and labelled. The 4 key hydroxyl moieties of RIF are highlighted in purple. Figure adapted from (10)

1.3 Rifamycin resistance

There are a number of ways bacteria can gain resistance to rifamycins. Target modification, efflux, and enzymatic inactivation have all been uncovered as mechanisms conferring resistance. Although target modification is currently the most commonly observed cause of clinical resistance, there are a number of genes involved in inactivating rifamycins that are of particular interest, due to their potential for mobility among bacteria. It is critical that we are aware of all the determinants comprising the rifamycin resistome in preparation for what may emerge into the clinic.

1.3.1 Target modification

A common resistance strategy employed by bacteria is the modification of the antibiotic target. This tactic is often used by antibiotic producers to avoid self harm. Target modification can occur in many ways, including mutation of the antibiotic target, production of an additional resistant target, altering transcription of the target, and many more. Resistance to rifamycins by target modification has been observed in a number of ways.

1.3.1.1 Point mutations in rpoB

Currently the leading cause of rifamycin resistance in the clinic is due to spontaneous point mutations in the target *rpoB*. Bacteria have a high propensity of developing resistance to rifamycins, which is why rifampin is always co-administered with other antibiotics (11,12). The region of RpoB where the majority of mutations occur is termed the rifamycin resistance determining region (RRDR) and is highly conserved across bacterial species (Figure 1.6). This explains the broad spectrum activity of this class of antibiotics. Mutations causing rifamycin resistance have been characterized in a number of species, including *Thermus aquaticus*,

Escherichia coli, and *Mycobacterium tuberculosis*. (Figure 1.6). The three most common sites of mutation are S455, H440, and D430 (*M. tuberculosis* numbering) (13). These residues are involved in binding rifampin directly, and mutations at these sites account for more than 85% of resistance mutations in tuberculosis. Mutations that are not involved in binding rifamycins nor occurring in the binding pocket can also cause resistance to rifamycins, and might be due to larger scale conformational changes in RpoB (10).

Mutations to RpoB are not without a fitness cost (14–16). This cost is different across the wide variety of mutations conferring resistance to rifamycins. With long enough exposure, additional mutations in the alpha and beta prime subunits of RNA polymerase can offset the fitness cost (16–18). Mutated RpoB was found to misregulate gene expression in a number of bacteria, and this feature of rifamycin resistant RNA polymerase has been exploited by microbiologists to activate expression of cryptic genes (19–22).

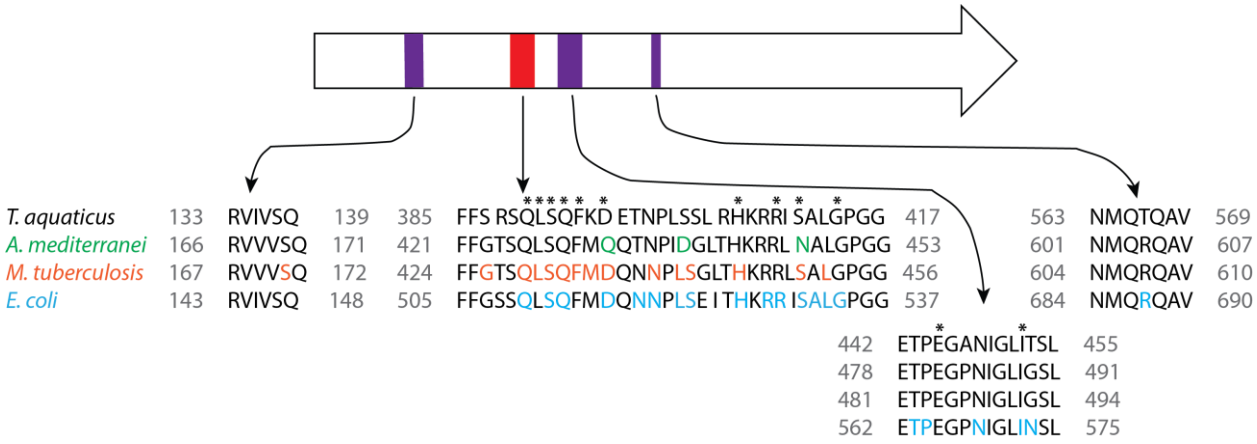

Figure 1.6. A comparison of bacterial *rpoB* genes. The regions highlighted in purple and red are highly conserved across bacterial species. The red region is called the rifamycin resistance determining region (RRDR) and is the most frequent site of mutations causing resistance. The residues directly involved in binding rifampin in the *T. aquaticus* crystal structure are marked with an asterisk. The coloured residues represent sites of common mutation in each species. Figure adapted from (10).

1.3.1.2 Duplication of rpoB

Some species of actinomycetes have been shown to contain more than one copy of *rpoB* in their genomes (23,24). The second copy of *rpoB*, sometimes called *rpoB2* or *rpoB(R)*, is located in a different region of the genome and harbours similar amino acid substitutions to classical resistant mutants of RpoB, hinting that this subunit confers rifamycin resistance; this was indeed found to be the case (24). Transcription of *rpoB2* was shown to coincide with transition into stationary phase and the commencement of secondary metabolism (23).

1.3.2 Efflux

Gram-negative bacteria are intrinsically less susceptible to rifamycins. This is in part due to the presence of the outer membrane, and in part a result of multidrug efflux pumps which act on hydrophobic compounds (25–28). *M. tuberculosis* has also been shown to upregulate several efflux pumps in the presence of rifamycins (29–32).

1.3.3 Enzymatic inactivation of rifamycins

Some opportunistic pathogens and several environmental bacteria are capable of inactivating rifamycins enzymatically. To date, four mechanisms of inactivation have been observed: ADP ribosylation, glycosylation, phosphorylation, and decomposition mediated by monooxygenation.

1.3.3.1 ADP Ribosylation

In 1987, Dabbs and coworkers identified that some bacteria were capable of inactivating rifamycins (33). ADP ribosylation was the first of these inactivation strategies to be fully characterized (34). This process was identified in fast growing *Mycobacterium* strains and a few

other environmental actinomycetes. The modified rifampin appeared to be ribosylated on the C23 hydroxyl group (35). As shown by structure activity relationships and the crystal structure of RNA polymerase, this hydroxyl residue is critical for bioactivity. Modification at the position causes a disruption of one of the key hydrogen bonds between the rifamycin scaffold and the target RpoB. This was the first instance of ribosylation as a mechanism of antibiotic inactivation. The gene responsible for rifamycin ribosylation was the *arr* gene, identified in *Mycobacterium smegmatis* (36). The *arr* gene was also shown to confer high level rifamycin resistance when heterologously expressed in *E. coli* (37) In 1999, a multidrug resistant strain of *Pseudomonas aeruginosa* was found to contain an integron with an *arr* homolog, named *arr-2* (38). Since then, *arr* genes have been found on integrons in many Gram-negative pathogens, including *Klebsiella pneumoniae*, *E. coli*, and *Acinetobacter baumannii* (39–42). This is particularly interesting because rifampin is rarely used in the treatment of these infections. Despite this, the association of the *arr* gene with other antibiotic resistance determinants has caused it to be maintained in Gram-negative pathogens.

ADP ribosyl transferases (ARTs) are well known to catalyze post-translational modifications in eukaryotes and modify a number of bacterial toxins (43). They do this by cleaving nicotinamide from NAD^+ and transferring the resulting ADP ribose group to the target protein. Although ARTs have many different protein targets, they share a common three-dimensional structure capable of binding NAD^+. Arr, despite being the only known example of a small molecule ribosyl transferase, shares a similar three-dimensional structure to eukaryotic ARTs (44). Despite being much smaller than the average ART, Arr represents the minimum structural motif required to bind NAD^+. Arr binds rifamycins in a deep substrate binding cleft, with a structural loop acting as a lid to keep the substrate in place once bound. There are no

interactions between amino acid side chains of Arr and the rifamycin scaffold; the drug is held in place entirely by a collection of backbone hydrogen bonds, water mediated interactions, and hydrophobic interactions.

Arrs are widespread among the environment and now the clinic. Several Arr enzymes from the environment were shown to be equivalent to the clinical *arr-2* at inactivating a number of rifamycin antibiotics (44). All known Arrs confer high level resistance to rifamycins. These enzymes are a classic example of transfer of environmental resistance determinants to the clinic and are exactly why we need to be continuously monitoring the resistome.

1.3.3.2 Glycosylation

In surveying environmental *Nocardia* species, Yazawa and coworkers uncovered that many were resistant to rifamycins, and identified the species *Nocardia brasiliensis* as being able to glycosylate rifampin (45). Structural studies showed that glycosylation occurs on the C23 hydroxyl, similarly to ADP ribosylation (46). By modifying the C23 hydroxyl, hydrogen bonding between the drug and its target is significantly disrupted. Since then, glycosylation of rifampin has been observed in a number of *Streptomyces* species, and has been attributed to the rifamycin glycosyltransferase gene *rgt* (47). Overexpression of *rgt* in *E. coli* confers high level resistance to a number of natural product and clinically used rifamycins (47).

Thus far, glycosylation as a mechanism of resistance has not emerged in the clinic, and is seen sparingly in the environment. Rgts are widespread among but confined to the Actinomycetales order of bacteria (47). The enzyme was found to use UDP glucose as a co-substrate and a source of glucose (47). Glycosyltransferases (GTs) are often found in biosynthetic clusters as tailoring enzymes for natural products. Rgt1438, isolated from a

Streptomyces species, shows strong similarity to GTs involved in glycopeptide tailoring, hinting that the origins of Rgts might be from other GTs involved in natural product biosynthesis (47). Currently, there is no crystal structure of an Rgt bound to a rifamycin substrate. This would be extremely beneficial in understanding specificity, activity, and history of these resistance determinants.

1.3.3.3 Phosphorylation

Phosphorylation of rifamycins was first described by Yazawa and coworkers in the species *Nocardia otitidiscaviarium*, followed by a number of *Nocardia, Streptomyces*, and *Bacillus* strains (48–51). Inactivation in *Bacillus* is particularly interesting, since many naturally occurring species are susceptible to rifamycins (50). Structural studies uncovered that phosphorylation occurs on the C21 hydroxyl group, which is critical for bioactivity (46). The gene encoding the rifamycin phosphotransferase, *rph*, was recently found in a *Streptomyces* species (51). These genes are widespread in the environment, and Rphs from a variety of sources confer high levels of resistance to rifamycins when overexpressed in *E. coli* (51).

The Rph enzyme represents a new family of antibiotic resistance proteins (52). Rphs are multidomain proteins that are similar to phosphoenol pyruvate synthase (PPSA). These enzymes are involved in gluconeogenesis, and utilize two separate active sites and three structural domains (53). ATP is bound by the ATP binding domain, and the beta phosphate is transferred to a His residue, releasing inorganic phosphate and AMP. The swivel domain then pivots to the second active site, on the pyruvate/PEP binding domain, where the transfer of the phosphate from His to pyruvate occurs, generating PEP (53). Rph is similar to PPSA in that it has three domains, including an ATP binding and a swivel domain. However, the swivel domain is located

in a different position, and in place of the pyruvate/PEP binding domain is a unique rifamycin binding domain, making Rphs a brand new family of enzymes (52).

As mentioned, *rph* genes are widespread among the environment. Of particular concern are *rph* genes within the genomes of pathogens such as *Bacillus anthracis, Bacillus cereus*, and *Listeria monocytogenes* (51). Yet these species appear to be sensitive to rifamycins, despite harbouring a bona fide resistance determinant. This is referred to as silent resistance, and in the appropriate genetic context these genes cause high levels of resistance to rifamycins (51). Likely, the original substrate for the Rph ancestor is something other than rifamycins, explaining their presence in these susceptible organisms. Recently, the crystal structure of Rph from *Listeria monocytogenes* has been solved in complex with rifampin (52). It appears that the rifamycin binding domain shows some weak structural similarity with enzymes involved in the phosphotransferase system in bacteria (52). These findings shed some light on the evolution of Rphs as antibiotic resistance mechanisms.

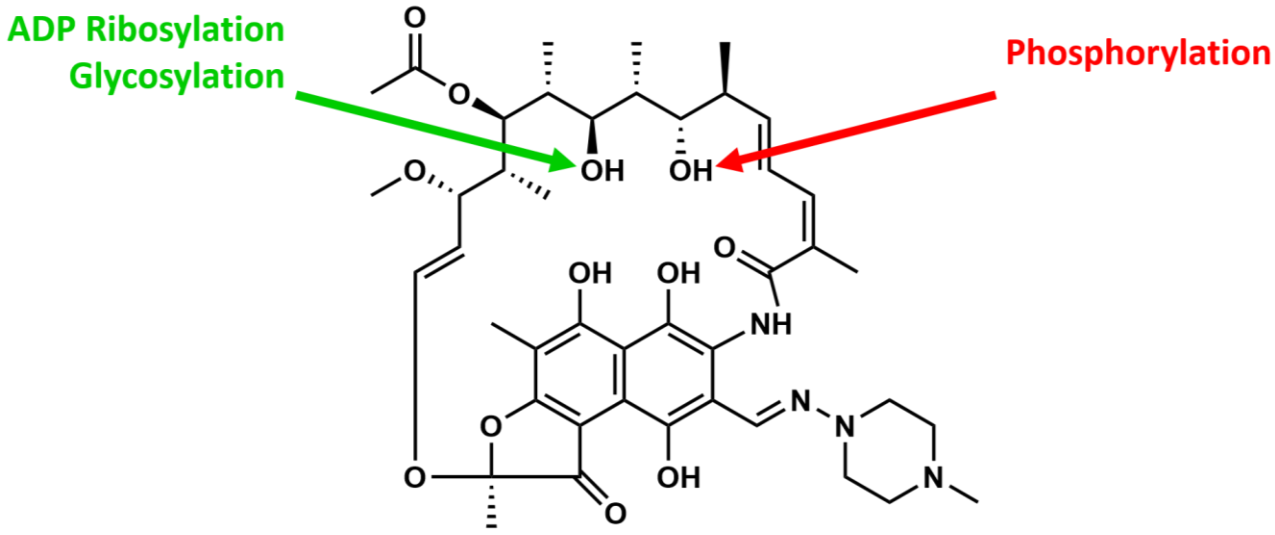

Figure 1.7 Sites of group transfer as a means for rifamycin resistance.

1.3.3.4 Decomposition mediated by monooxygenation

Decolourization of rifamycins was first observed by Dabbs and coworkers in 1987 in species of *Rhodococcus equi* (33). Attempts to isolate the decolourized rifamycin compound were unsuccessful, and Tanaka and coworkers suggested this was because the molecule decomposes into smaller fragments (48). In 1997, Andersen and Dabbs created a genomic library for *Rhodococcus equi* and screened for the decolourization phenotype. This search returned an open reading frame which they called the *iri* gene (54). *Iri* had high sequence similarity to phenolic monooxygenase genes, suggesting that it may modify the aromatic core of the rifamycin scaffold, but no follow up characterization of the protein was performed (54). In 2010, a homolog of the *iri* gene was found in a *Nocardia* species and subsequently renamed the *rox* gene (55). Hoshino and coworkers overexpressed this gene in *E. coli*, and used these cells to generate and purify a monooxygenated form of rifampin. However once again, no studies of the Rox protein itself were performed. They propose that the hydroxylation occurs on the N2' of the semisynthetic tail of rifampin (Figure 1.8) (55). Interestingly, this part of the molecule is not involved in binding to RpoB (10), and is not present in a number of rifamycin antibiotics.

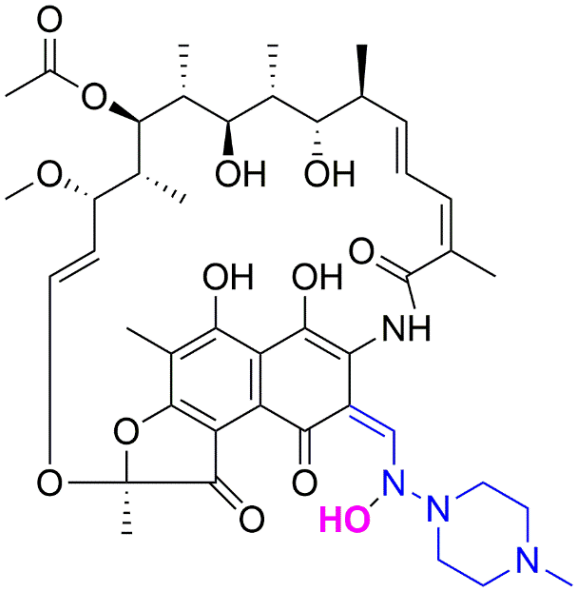

Figure 1.8 The proposed structure of monooxygenated RIF by Hoshino and coworkers. The semisynthetic tail of RIF is highlighted in blue, and the additional oxygen moiety in pink.

1.3.3.5 Regulation of enzymatic inactivation

Antibiotic resistance is often associated with some fitness cost. For this reason, many bacteria have developed mechanisms of responding to antibiotic stress with the induction of resistance. Recently a genomic analysis was performed on regions of DNA surrounding rifamycin inactivating genes, in an effort to find some sort of conserved genetic machinery (51). A highly conserved palindromic motif was found upstream of all known rifamycin inactivating genes within the order Actinomycetales (Figure 1.9) (51). This palindrome, termed the rifamycin associated element (RAE) was found to be key in inducing expression in response to rifamycins through initial transcriptional fusion experiments (51). The effector responsible for this RAE specific induced transcription remains unknown.

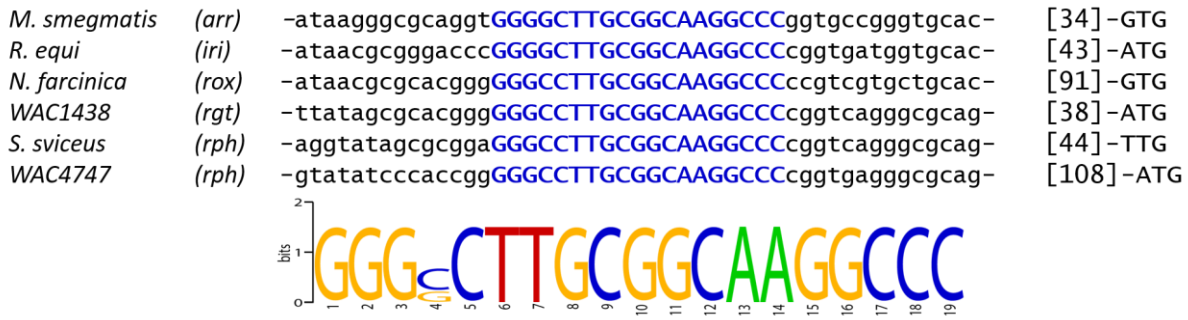

Figure 1.9 Regions containing the RAE from various Actinomycetes. On the left is the species in which the RAE is found, followed by the rifamycin resistance gene that the RAE precedes. On the right in square brackets is the distance from the RAE containing region shown to the start codon. Figure adapted from (51).

1.4 Research Objectives

The rifamycins are an increasingly important class of antibiotics in an era of antibiotic resistance. Once reserved for the treatment of *Mycobacterium tuberculosis*, rifamycins are experiencing renewed usage in treatment of other multidrug resistant organisms. Their wide range and amenability to semi synthesis makes rifamycins good candidates for development of new generations of antibiotics. It is reasonable to speculate that as they become more widely used, rifamycin resistance will also become more common. Bacteria in the environment have had millions of years to devise strategies to inactivate rifamycins. By understanding these mechanisms, we can anticipate new resistance determinants before they are mobilized into the clinic.

Genes conferring rifamycin resistance are widespread in the environment. They appear to be regulated in some way by a small DNA sequence motif, the rifamycin associated element (RAE). The RAE is found upstream of rifamycin resistance genes. Using a rudimentary reporter assay involving expression of a kanamycin resistance cassette, Spanogiannopoulos showed that

in response to low levels of rifamycins, a promoter region containing the RAE induces gene expression (51). Exactly how this process works remains unknown.

The RAE containing region used in the initial reporter was from WAC4747, an environmental isolate from the Wright Actinomycetes Collection at McMaster University. However, in order to study the RAE in the future, it would be ideal to use a more genetically tractable organism. *Streptomyces venezuelae* is an increasingly popular model organism for *Streptomyces* genetics. A search of the *S. venezuelae* genome revealed 3 RAE; one of these is upstream of a *rox* gene. Neither the RAE nor the Rox enzyme are well understood. The objective of this thesis is then twofold: characterize Rox to study the still poorly defined process of rifamycin decomposition initiated by monooxygenation, and confirm that the RAE induces gene expression in *S. venezuelae* in the same way as it did in WAC4747.

Regions containing the RAE from *S. venezuelae* were cloned into a reporter and assayed for their ability to respond to rifamycins and induce transcription. The reporter strains generated in this work will be used in future studies on the RAE. The *rox* gene from *S. venezuelae* was overexpressed, purified, and characterized *in vitro*. Rox was previously predicted to be an FAD dependant monooxygenase based on sequence similarity to well characterized representatives of this class. This was confirmed by the crystal structure of Rox. Steady state kinetics and MIC data was obtained for Rox. The product of the *in vitro* reaction was purified, and the structure elucidated by NMR analysis. Taken together, a reaction mechanism can be proposed for Rox, representing a novel mechanism of antibiotic resistance.

Chapter 2. Characterizing the RAE in *Streptomyces venezuelae*

2.1 Introduction

The environment is a large source of bacterial diversity (56). Due to the sheer number of species that inhabit the soil, bacteria have had to devise methods of communication, signal transduction, and antagonism. Antibiotics are widely produced by microorganisms, and one of their functions is to act as a form of chemical warfare in the environment (2). As such, bacteria have also devised strategies to become resistant to the harmful effects of antibiotics. Target modification, active efflux, and inactivation all serve in the bacterial toolbox for resistance. Antibiotic resistance mechanisms are generally associated with a fitness cost to the cell (2); it is therefore advantageous for bacteria to have control over the expression of resistance. One way of doing this involves sensing the presence of an antibiotic and responding by expressing resistance determinants. One example of this would be the TetR system, where the transcription of tetracycline efflux pumps is normally repressed by the repressor TetR (57). However, in the presence of tetracycline, TetR undergoes a conformational change resulting in release from the promoter region and the resistance gene is expressed (57). In this way it appears bacteria have evolved to only express costly resistance genes when it is necessary.

Rifamycin antibiotics target bacterial RNA polymerase. A number of rifamycin resistance determinants have been identified in the environment. Despite the simplicity of target modification as a means of resistance, genes involved in ADP-ribosylation, glycosylation, phosphorylation, and monooxygenation of rifamycins are widespread among environmental bacteria. In 2014, a conserved genetic element was found to be associated with genes conferring

enzymatic resistance to rifamycins (51). The rifamycin associated element (RAE) is a highly conserved, 19 bp palindromic sequence identified upstream of a number of confirmed resistance genes (Figure 1.9) (51). Interestingly, the RAE appears to be involved in rifamycin-induced gene expression. When tested using a rudimentary reporter assay involving expression of a kanamycin resistance cassette, the region of DNA containing the RAE was capable of inducing kanamycin resistance in response to rifamycins (Figure 2.1). This was not the case when the palindrome was disrupted, nor when this reporter construct was introduced into non-actinomycetes. It would appear the RAE is involved in some inducible rifamycin resistance process in the environment, although exactly how this process works remains unclear.

The RAE is widespread among Actinobacteria. The DNA used in this initial reporter assay was that of WAC4747, a *Streptomyces* species from the Wright Actinomycetes Collection. However, in order to study the induction of rifamycin resistance and what role the RAE has to play, a more genetically tractable host is desirable. The species *Streptomyces venezuelae* is a well characterized organism for studying *Streptomyces* genetics (58). In this work, we probed *S. venezuelae* for the presence of the RAE and the ability of this genetic element to induce gene expression. We chose to use the well characterized reporter plasmid pGUS for *Streptomyces*. This reporter utilizes a β-glucuronidase gene fused to the promoter of interest, and cleaves a chromogenic substrate to generate a blue precipitate as a readout. The reporter constructs and strains generated in this work will be used in future studies to elucidate the mechanism of rifamycin-induced transcription in Actinomycetes.

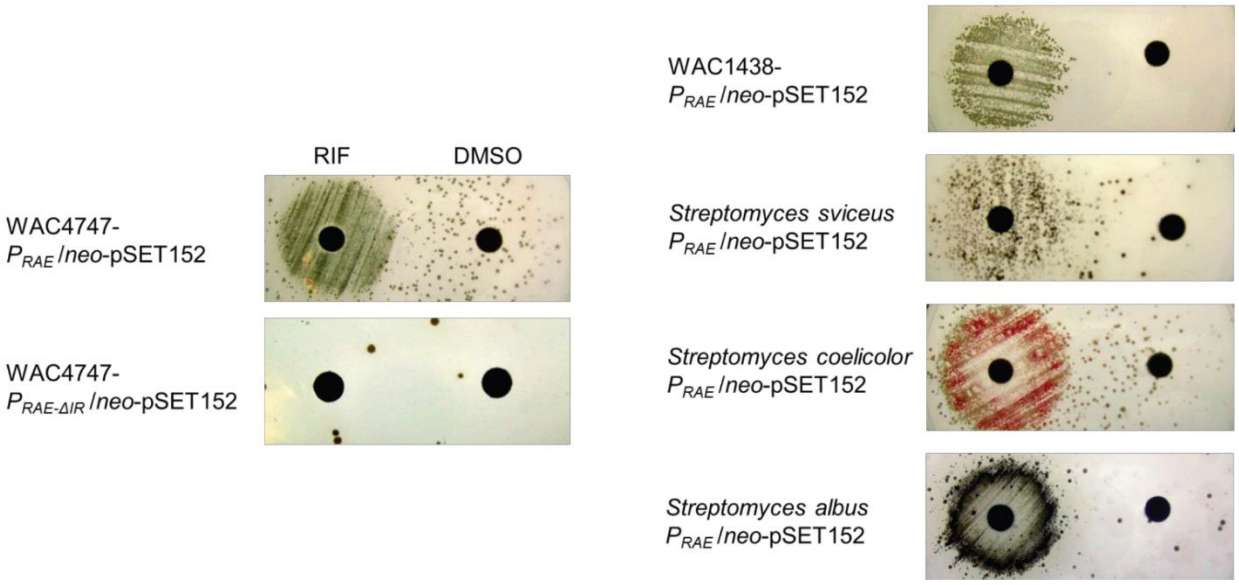

Figure 2.1 Kanamycin reporter assay performed by Spanogiannopoulos. P_{RAE}/neo-pSET152 is the reporter plasmid with the RAE containing region fused to a kanamycin resistance cassette. Growth was induced on kanamycin containing media by RIF in each of the five Actinomycetes tested. WAC4747-$P_{RAE-\Delta IR}$/neo-pSET152 is a negative control in which the RAE was replaced by a sequence of 19 random nucleotides. DMSO is a vehicle control. Figure adapted from (59).

2.2 Materials and methods

2.2.1 Identifying and cloning of RAE containing regions in S. venezuelae to generate reporter constructs

The genome sequence of *S. venezuelae* ATCC 10712 was searched using blastn with the RAE sequence (GGGGCTTGCGGCAAGGCCC) as a query. Three close matches were identified; each was examined for its validity based on genetic context. The region of DNA to be cloned was extended on either side of the RAE to the terminus of the next open reading frame, as illustrated in Figure 2.2. Regions of DNA were amplified from *S. venezuelae* genomic DNA by PCR. The primers used to amplify each region are listed in Appendix 1. The sizes of PCR product ranged between 200- 250 bp. The amplified promoter regions were cloned into the pGUS plasmid using *Kpn*I and *Xba*I restriction enzymes, creating a transcriptional fusion to the β-glucuronidase gene *gusA* (60). Constructs were transformed into chemically competent TOP10 *E. coli* cells and sent for sequencing at the MOBIX facility at McMaster University.

2.2.2 Cloning of RAE associated genes and rifampin MIC determinations

To examine whether the three genes associated with the RAE conferred resistance to rifamycins, they were cloned into *E. coli* strain BL21 (DE3). Each gene was amplified by PCR using primers Rox_F/R, Rgt_F/R, and Hel_F/R (Appendix 1). The PCR products were cloned into the pET28a using *Nde*I and *Bam*HI. Constructs were sequenced to confirm the correct inserts at the MOBIX facility at McMaster University. Constructs were transformed into chemically competent *E. coli* BL21 (DE3) cells for minimum inhibitory concentration (MIC) experiments. MICs were determined for rifampin according to the CLSI standard broth microdilution method (61) with 1 μM IPTG added to induce expression of the genes.

2.2.3 Generation of reporter strains of S. venezuelae

Reporter constructs were transformed into chemically competent *E. coli* ET12567-pUZ8002 competent cells for conjugation into *S. venezuelae.* Conjugations were performed as described by Kieser (62). Transconjugants were selected by growth on 50 µg/mL apramycin and confirmed by PCR amplification. Strains of *S. venezuelae* containing positive and negative pGUS reporter constructs were a gift from Dr. Marie Elliot at McMaster University.

2.2.4 Chromogenic reporter assay for β-glucuronidase activity

Each of the five reporter strains of *S. venezuelae* and wild type were grown in liquid SIM for 48 h. A Bennett's agar plate was flooded with 400 µg in 1 mL of 5-bromo-4-chloro-3-indolyl β-D-glucuronide (X-Gluc) and allowed to dry. The liquid culture was used to streak a line of bacteria onto the plate with a disk in the middle, containing either 500 µg rifampin, 100 µg vancomycin, or 10 µL 20% DMSO. Plates were incubated for 48 h at 30 °C wrapped in foil before imaging.

2.3 Results

2.3.1 The RAE in S. venezuelae and their associated genes

We searched the genome of *S. venezuelae* ATCC 10712 for the RAE using blastn. Two exact matches and one with two mismatches at the end were identified. The locations and genetic context of these elements are listed in Table 2.1, and illustrated in Figure 2.2.

Table 2.1 Locations of the RAE in *S. venezuelae* ATCC 10712

RAE location	Complement?	Mismatches to query	Nearest 5' ORF	Nearest 3' ORF
519,605 - 519,623	No	0	Amidase	Rifampin monooxygenase
6,165,400 - 6,165,418	Yes	0	Putative helicase	Beta-lactamase class C and other penicillin binding proteins
3,760,571 - 3,760,587	No	2	Hypothetical protein	Hypothetical protein

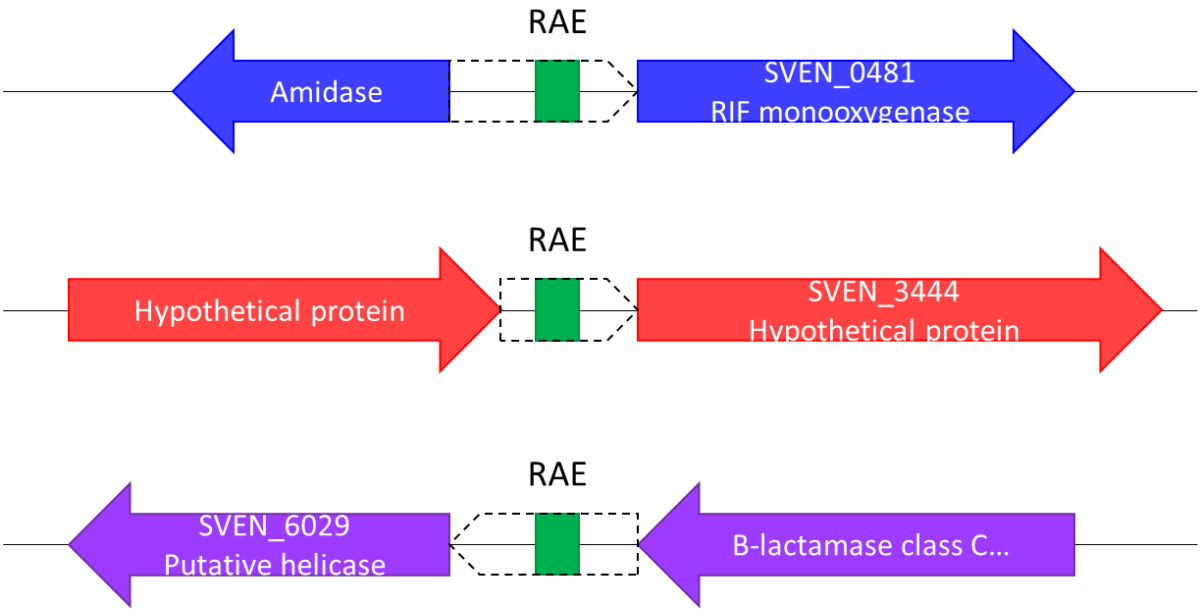

Figure 2.2 Genetic context of the three RAE in the *S. venezuelae* genome.

As shown in Figure 2.2, one of the RAEs is upstream of an annotated rifampin monooxygenase, and another is upstream of a putative helicase. These types of genes are frequently found to be associated with the RAE (51). One of the genes encoding a hypothetical protein adjacent to the 2 bp mismatched RAE shows 62% identity to a known *rgt* and 75-81% identity to other putative glycosyltransferase genes. To see if any of these genes conferred resistance to rifamycins, each was cloned into *E. coli* BL21 (DE3) and the MIC for rifampin was determined (Table 2.2). The rifampin monooxygenase *rox* conferred a 4-8-fold MIC increase, however neither the helicase nor the putative glycosyltransferase conferred any resistance in this context. Nevertheless, we decided to clone all three regions containing the RAE into our reporter construct.

Table 2.2 Rifampin MICs for *E. coli* BL21 (DE3)

Strain	MIC (µg/mL)
BL21-pET28a	4
BL21-pET28a-rox	16-32
BL21-pET28a-helicase	4
BL21-pET28a-putative rgt	4

2.3.2 Generating the S. venezuelae β-glucuronidase reporter strains

The reporter we chose to use was the pGUS plasmid, designed specifically for use in Actinomycetes. The plasmid contains a promoterless β-glucuronidase gene *gusA* which can be fused to the promoter of interest, seen in Figure 2.5. When expressed, *gusA* cleaves β-glucuronides, and a β-glucuronide linked substrate can be used to generate the desired readout format (chromogenic, spectrophotometric, etc) (60). We chose to clone the entire region between the two ORFs flanking the RAE into our reporter construct (Figure 2.2). The promoter regions from *S. venezuelae* containing the RAE were amplified by PCR and cloned into the pGUS

plasmid (Table 2.3). The constructs were sent for sequencing to confirm successful insertion of promoters before transforming into *E. coli* ET12567-pUZ8002. This strain of *E. coli* is commonly used for bi-parental conjugation into *Streptomyces* species. The pGUS plasmid integrates into the genome. The reporter constructs were conjugated into *S. venezuelae* and successful transconjugants were confirmed by PCR. Strains of *S. venezuelae* already containing positive and negative pGUS reporter constructs were a gift from the Elliot lab at McMaster University. The negative control simply contains *gusA* with no promoter, and the positive control contains a *gusA-ermE** fusion, where *ermE** is a *Streptomyces* constitutive promoter. The generated and acquired reporter strains of *S. venezuelae* used are listed in Table 2.4.

Table 2.3 Promoters cloned into the pGUS reporter plasmid

Promoter name	Upstream of:	Genomic Location
Prox	Rifampin monooxygenase	519,476 - 519,682
Phel	Putative helicase	6,561,340 - 6,561,553
Prgt	Hypothetical protein	3,760,445 - 3,760,696

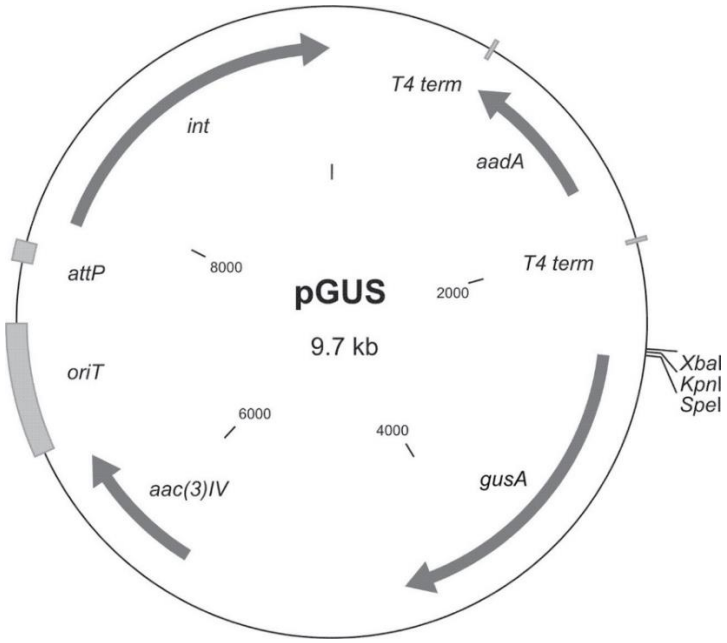

Figure 2.3 The pGUS reporter plasmid. The multiple cloning site upstream of *gusA* is used to create transcriptional fusions. Plasmid map from (60).

Table 2.4 Names of reporter strains of *S. venezuelae* generated

Strain name	Promoter	Contains a RAE?
S. venezuelae- pGUS	None	No
S. venezuelae- pGUS-ermE*	ermE*	No
S. venezuelae- pGUS-Prox	Prox	Yes
S. venezuelae- pGUS-Phel	Phel	Yes
S. venezuelae- pGUS-Prgt	Prgt	Yes (17/19)

2.3.3 β-glucuronidase assay findings

To study whether the promoter regions containing the RAE from *S. venezuelae* induce transcription in response to rifamycins we used the pGUS reporter plasmid, creating a transcriptional fusion to the β-glucuronidase gene *gusA*. We chose to use a chromogenic assay, where the substrate X-Gluc contains a glucuronic acid sugar linked by a β-glucuronide bond to a halogenated indole that when cleaved from the sugar forms a blue precipitate. The *gusA* product cleaves this bond, and in this way blue colour can be observed as an indicator of expression (60). We tested each of our reporter strains for their β-glucuronidase activity in the presence of rifamycins. Our hypothesis was that the strains containing the RAE promoters would express *gusA* only in response to rifamycins, while the positive control should express *gusA* constitutively and the negative control should never express *gusA*. We also tested whether vehicle alone could induce expression, and whether other antibiotic stress in the form of vancomycin induced expression. The results can be seen in Figure 2.4. The controls reacted as expected, where blue precipitate was formed constitutively around the positive control, and not at all in the negative control. *S. venezuelae*- pGUS- Prox expresses *gusA* only in response to rifamycins as hypothesized, which can be observed by the small zone of blue precipitate at the edge of the Prox streak near the RIF diffusion zone. Neither *S. venezuelae*- pGUS- Prgt nor *S. venezuelae*- pGUS- Phel seems to respond to RIF. In fact, *S. venezuelae*- pGUS- Prgt also

appears to constitutively express *gusA*, while for *S. venezuelae*- pGUS- Phel it does not look like any *gusA* is expressed after 48 h.

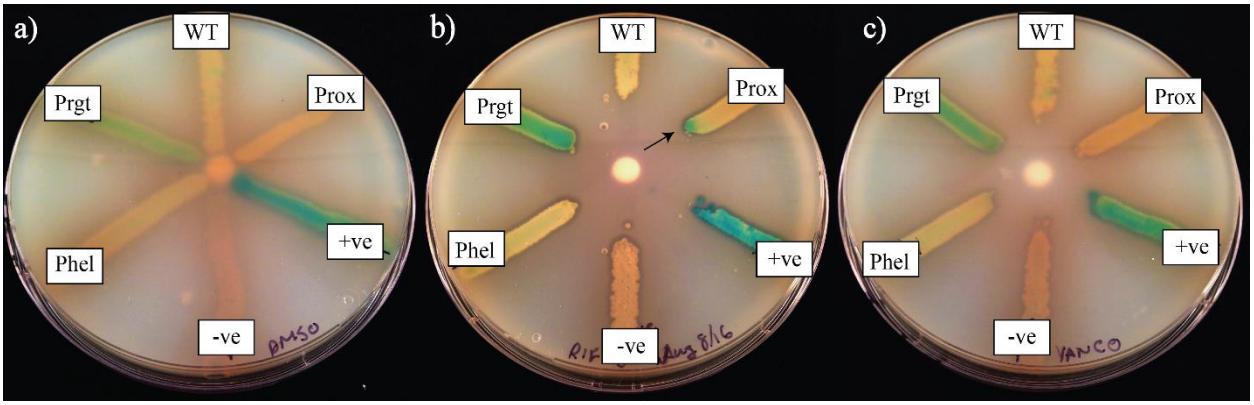

Figure 2.4 β-glucuronidase assay of *S. venezuelae* strains. a) Vehicle control, b) RIF, c) Vancomycin. The strains are labelled around the edge of the plate. In b) the blue precipitate can be observed at the edge of the RIF diffusion zone only in the Prox streak, indicated by an arrow.

2.4 Discussion

Rifamycin resistance by enzymatic inactivation is widespread in the environment. The RAE is a conserved genetic element associated with genes conferring rifamycin resistance, and appears to be inducible by rifamycins. How the RAE induces transcription in the presence of rifamycins remains unknown. To study this, detailed genetic analysis will need to be performed. Currently, only the RAE from WAC4747 has been characterized as responding to rifamycins; this species is from an in house collection at McMaster University. Ideally for more detailed genetic studies, we would use an organism that is well characterized and widely used. *S. venezuelae* is a relatively new model organism for *Streptomyces* genetics; it is attractive for a number of reasons, including a short growing time and its ability to sporulate in liquid media (58). For this reason, we decided to move our downstream studies of the RAE into *S. venezuelae*.

In probing the genome of *S. venezuelae*, we found two perfect matches to the RAE. They were found in intergenic regions as expected. One was located upstream of an annotated rifamycin monooxygenase, and one was upstream of a putative helicase. Both of these have been previously found to be associated with the RAE (51). There was also a 2 bp mismatched RAE upstream of a hypothetical protein, sharing 62% identity with known glycosyltransferase *rgt1438* (47). It was intriguing to find a potential rifamycin monooxygenase and glycosyltransferase in the genome, since *S. venezuelae* has a very low MIC for rifampin. When overexpressed in *E. coli*, the monooxygenase increased the MIC for rifampin 4-8-fold, while the glycosyltransferase and helicase did not confer any resistance; however it is unclear whether these genes are being expressed in the *E. coli* background. It remains to be seen whether the glycosyltransferase is a functional rifamycin glycosyltransferase, while characterization of the monooxygenase is described in Chapter 3.

Regions of DNA containing the RAE between adjacent open reading frames were cloned into the reporter plasmid pGUS; these reporter constructs were then conjugated into *S. venezuelae*. This generated a transcriptional fusion of the promoter region of interest to the β-glucuronidase gene *gusA* for detection using a chromogenic assay. The positive and negative control strains behaved as expected as illustrated in Figure 2.4. The Prox promoter showed the same phenotype as the WAC4747 reporter, in which expression was induced only in the presence of low levels of RIF. Interestingly, neither the Prgt nor Phel promoters showed this phenotype; the Prgt promoter appears constitutive, while it is difficult to tell with the Phel promoter. The Phel promoter contains a RAE exactly matching that of the Prox promoter, while the Prgt promoter contains 2 bp mismatched from the Prox RAE. The *rox* gene was the only one of the three that conferred rifamycin resistance; logically it makes sense that this gene should be induced by the presence of rifamycins. There must be something other than just the palindrome that determines gene expression in response to rifamycins.

How expression is induced by the RAE in the presence of rifamycins remains a mystery. Many unsuccessful attempts were made in the past to pull out the effector of the RAE from WAC4747. Going forward, studies can be carried out in *S. venezuelae* knowing that the RAE upstream of the rifampin monooxygenase is induced in the presence of rifamycins. *S. venezuelae* is well studied; the genome sequence and RNA sequencing data is available. In the future, RNA sequencing experiments could be performed in the presence of low levels of rifampin to try and determine the effector of the RAE.

Chapter 3. Characterizing the rifamycin monooxygenase Rox

3.1 Introduction

Rifamycins are a unique class of antibiotic that act as RNA polymerase inhibitors. Natural product rifamycins like RIF-SV provide the scaffold, and semisynthetic derivatives including rifampin (RIF) have become frontline agents in the treatment of *Mycobacterium tuberculosis*. The environment is a wide reservoir of novel antibiotic resistance mechanisms, and rifamycin resistance is no exception. Environmental isolates have been found to inactivate rifamycins enzymatically in a number of ways. Genes encoding rifamycin ribosyltransferases (34), glycosyltransferases (47), and phosphotransferases (51) were all discovered in the environment and shown to be effective resistance determinants. The *arr* gene, responsible for ADP-ribosylation of rifamycins, has already been mobilized from environmental hosts to clinically relevant pathogens like *Pseudomonas, Klebsiella,* and enterobacterial species (38–42). It is therefore critical that we study the mechanisms of rifamycin resistance in the environment to be prepared for their potential migration to the clinic.

The decomposition of rifamycins is a phenomenon that has been observed in some environmental Actinomycetes but is not well understood. In 1987 Dabbs and coworkers first observed the decolourization of rifampin in *Rhodococcus erythropolis* (33). When attempts to purify the decolourized rifampin failed, it was suggested that perhaps the decolourization was due to degradation of the drug (48). The gene responsible for decolourization in *R. erythropolis* was eventually identified as *iri* (inactivation of rifampin) by a functional genomics approach (54). In 2010, Hoshino and colleagues identified a homolog to *iri* in *Nocardia farcinica*, called

rox (rifampin monooxygenase). The group proposed a structure of monooxygenated RIF (RIF-O), but they did so using cells without ever studying the Rox enzyme itself. Very little is known about the monooxygenation mediated decomposition of rifampin.

The *rox* gene sequence was determined by Andersen and coworkers (then called *iri*) (54). They proposed that Rox is a flavin dependent monooxygenase, due to high sequence similarity to other monooxygenases involved in natural product biosynthesis or aromatic hydroxylation (54). They postulated that Rox may act on the aromatic core region of rifamycins due to the similarity to these enzymes. However, when Hoshino and coworkers proposed RIF-O as the product of the Rox reaction, the hydroxylation was shown on the synthetic tail of the RIF molecule. This directly contradicted the idea that Rox acts on the aromatic core. It also begs the question as to how Rox might modify other rifamycins with different tail regions. Without direct assessment of the enzyme, this remains unclear.

Flavin-dependent monooxygenases (FMOs) have been well studied. There are eight major classes of FMOs; these classes are dependent on a number of factors including enzyme structure, type of flavin, electron donor, and the reaction they catalyze (63). Rox shows high sequence similarity to members of Group A FMOs, the FAD-dependent monooxygenases, which are enzymes encoded by a single gene and utilizing FAD and NAD(P)H as an electron donor (63). These enzymes are also sometimes referred to as aromatic hydroxylases for their tendency to have aromatic substrates. One of the most well studied examples of an aromatic hydroxylase is *para*- hydroxybenzoate hydroxylase (pHBH), which catalyzes the hydroxylation of *para*-hydroxybenzoate, as shown in Figure 3.1 (64).

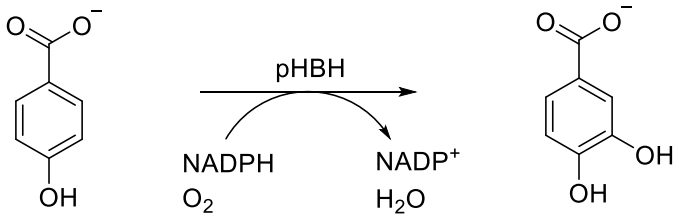

Figure 3.1 The reaction catalyzed by pHBH.

The kinetic mechanism of pHBH has been studied extensively, and is a prototype for FAD dependent monooxygenase reactions (64). These enzymes act by electrophilic aromatic substitution mechanism presented in Figure 3.2. First, substrate binding initiates the rapid reduction of the FAD cofactor by the electron donor NAD(P)H. The reduced flavin then reacts with molecular oxygen to form C(4a)-hydroperoxyflavin. The distal oxygen of this C(4a)-hydroperoxyflavin then acts as the electrophile in the aromatic substitution, with the aromatic substrate acting as the nucleophile. In pHBH, specific amino acid residues are involved in deprotonation of the phenol group, increasing the nucleophilic tendency of the substrate. The transfer of one oxygen from the C(4a)-hydroperoxyflavin to the *ortho*- position of hydroxybenzoate breaks the peroxide bond of the cofactor. The product readily isomerizes to the final 3,4-dihydroxybenzoate, and the hydroxyl group bound to the flavin is released as a water molecule. The crystal structure of pHBH has been solved, along with a number of other hydroxylases involved in aromatic degradation and the biosynthesis of natural products (65–68). These enzymes are characterized by an NAD binding (NADB) Rossmann fold within the FAD binding domain.

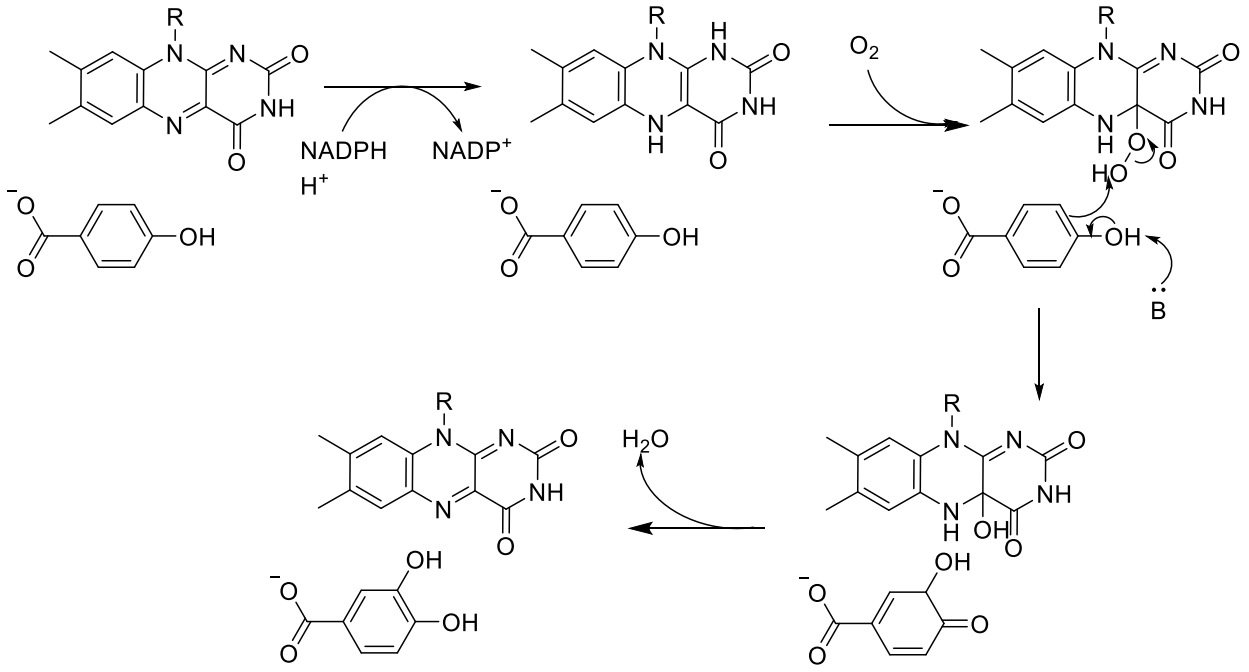

Figure 3.2 The electrophilic aromatic substitution mechanism of pHBH.

Degradation initiated by monooxygenation of an antibiotic as a means of resistance has been observed previously in the case of the tetracycline monooxygenase TetX (69). TetX is a flavin dependent monooxygenase but is not an aromatic hydroxylase. TetX requires oxygen and NADPH to hydroxylate tetracycline, which proceeds to cause spontaneous, non-enzymatic breakdown of the molecule (69).

In this work, Rox from *S. venezuelae* was biochemically characterized to elucidate the molecular mechanism. This includes overexpression and purification of the enzyme for protein crystallography, enzyme kinetics, and examination of the *in vitro* reaction products.

3.2 Materials and methods

3.2.1 Investigation of rifamycin degradation in S. venezuelae

To determine whether *S. venezuelae* was degrading rifamycins, cultures of *S. venezuelae* were inoculated in liquid SIM and grown for 48 h at 30 °C. After 48 h, cultures were inoculated with 25 µg/mL either RIF or RIF-SV. Cultures were grown for 48 h more, taking aliquots every 12 h. Aliquots were mixed with an equal volume methanol and spun for 10 min at 13 000 xg before running on a C18 column on the Applied Biosystems QTRAP liquid chromatography mass spectrometry system. Samples were separated using the following method:

Total time (min)	Flow rate (µL/min)	Solvent A (%)	Solvent B (%)
0.0	1000	90	10
1.0		90	10
7.0		3	97
8.0		3	97
8.5		90	10
9.0		90	10

where solvent A is water with 0.05% formic acid, and solvent B is acetonitrile with 0.05% formic acid.

3.2.2 Cloning, overexpression and purification of Rox

The *rox* gene was amplified by PCR from the genome of *S. venezuelae* using the primers Rox_F and Rox_R (Appendix 1). The size of the PCR product coincided with the expected size of the gene, approximately 1.4 kb. The amplified gene was cloned into the pET28a(+) expression vector using restriction enzymes *Nde*I and *Bam*HI, creating an N-terminal His-tag. The construct was transformed into chemically competent *E. coli* BL21(DE3) cells for overexpression and purification. A single colony was used to inoculate a starter culture of 10 mL of LB containing 50 µg/mL kanamycin. This was grown for approximately 18-20 h before the 10 mL starter

culture was used to inoculate 1 L of LB containing kanamycin. The 1 L culture was grown at 37 °C with 225 rpm shaking until the optical density at 600 nm (OD_{600}) was 0.4. Expression was induced by adding 400 μM IPTG, and cultures resumed shaking at 225 rpm and 16 °C for an additional 16-20 h. Cells were pelleted by centrifugation at 8,000 x g for 20 min and stored at -80 °C. Cells were thawed and resuspended in buffer A (50 mM HEPES (pH 7.5), 100 mM NaCl, 50 mM imidazole) for cell lysis. Lysozyme and DNase were added to the resuspension and incubated on ice for 30 min before cell lysis by a Constant Systems continuous-flow cell-disruptor. Cell lysate was centrifuged for 30 min at 4 °C and 20,000 x g to remove cell debris. The supernatant was loaded into a 50 mL super-loop to load onto a GE 5 mL HisTrap FF nickel column using a GE AKTA Purifier system. Protein was eluted using a linear gradient from 0-100% buffer B (50 mM HEPES (pH 7.5), 100 mM NaCl, 1 M imidazole) over 20 min. Fractions of 1 mL volume were collected and analyzed by SDS-PAGE, and those containing Rox were pooled and dialyzed overnight at 4 °C against 2 L of dialysis buffer (25 mM HEPES (pH 7.5), 300 mM NaCl). Glycerol was added to dialyzed protein to 20 % glycerol and stored at -20 °C for long term storage, or kept at 4 °C for short term storage.

3.2.3 Purification of Rox for crystallization trials

The *rox* gene was subcloned from pET28a into the vector pET19Tb (pET19b with a tobacco etch virus (TEV) cleavage site in place of the enterokinase site) using the restriction enzymes *Nde*I and *Xho*I. This vector contains a TEV protease cleavage site between the N-terminal His-tag and the *Nde*I cut site which can be used to remove the His-tag before crystallization. The pET19Tb construct was transformed into chemically competent *E. coli* BL21(DE3) cells for expression and purification, as previously described in section 3.2.2. Dialyzed protein was transferred to a flask and TEV protease was added. This was incubated at

12 °C at 100 rpm shaking for 8 h, before adding an second aliquot of TEV protease and continuing to incubate for 16 h. Approximately 2 mL of nickel NTA resin in dialysis buffer was added to the flask before rocking at 4 °C for 30 min. The slurry was then poured into a gravity column. The flow through containing Rox without a His tag was collected and analyzed by SDS-PAGE. The protein solution was concentrated to 2 mL for purification using a GE HiPrep S200 (26/20) gel filtration column. This was carried out at 4 °C, and fractions containing Rox were pooled and dialyzed against 2 L dialysis buffer.

3.2.4 Crystallization of Rox

Rox without a His-tag was purified as described in section 3.2.3. The protein was concentrated to ~ 30 mg/mL using a centrifugal filter unit with a molecular weight cut-off of 30 kDa. Overall, 192 crystallization conditions were screened for optimal crystal growth, using the commercially available Qiagen Classics and Classics II screening suites. Equal volumes of protein solution and well solution were mixed to a final volume of 0.6 µL. Conditions were screened using the sitting drop vapour diffusion method; the trays were incubated at room temperature in a Formulatrix Rock Imager 182 incubator and imaged automatically after 12 h, and then every 24 h for one week. Initial hits from the screen were further optimized by fine screening using the hanging drop vapour diffusion method. This fine screening systematically varied conditions significant in crystallization, including pH and percentage polyethylene glycol. Buffer pH was varied up to ± 1.5 pH unit, and polyethylene glycol (PEG) concentration was varied up to ± 15%.

Rox was infused with rifampin to obtain crystals with bound substrate. A solution of 1.4 mM RIF was added to 4 mL of buffer and incubated with 1.4 mM Rox on ice for 20 min. A centrifugal filter unit was used to remove buffer. This process was repeated twice more until the

protein was assumed to be saturated with RIF. After concentrating the RIF infused Rox was used to set hanging drop trays.

For data collection, crystals were transferred to mother liquor containing 20% glycerol as a cryoprotectant. Data was collected at 100 K with Cu Kα X-rays generated by a Rigaku 007 Microfocus rotating-anode generator equipped with VariMax HF optics and a Rigaku Raxis IV2+ detector. All X-ray data was reduced with HKL-3000 software. A model for molecular replacement was generated using Phenix.ensembler. The aromatic hydroxylases PgaE (PDB code 2QA1), CabE (PDB code 2QA2), and OxyS (PDB code 4K2X), and both available structures of the atypical Baeyer-Villiger monooxygenase MtmOIV (PDB codes 4K5S and 3FMW) were used to create an ensemble for molecular replacement using the PDB structures and multiple sequence alignment. This ensemble was used by Phenix.phaser to generate a structure of Rox, which was then refined using Phenix.refine. X-ray data collection and analysis was performed by Dr. Georgina Cox in the Wright Lab.

3.2.5 Site directed mutagenesis of Rox

Site directed mutagenesis of the *rox* gene was performed with KAPA high fidelity polymerase and primers c138g_F and c138g_R (Appendix 1). Each PCR reaction contained the following: 1 ng of pET28a-*rox* plasmid template, 0.3 µM of each primer, 3% DMSO, and 1 U KAPA. The reaction was performed in a Bioer LifeEco thermal cycler using the following method:

Cycle step	Temperature (°C)	Time	Number of cycles
Initial denaturation	98	1 min	1
Denaturation	98	20 s	35
Annealing	65	15 s	
Extension	72	4 min	
Final extension	72	7.5 min	1

Two microliters of *Dpn*I was added to the PCR product and incubated for 1 h at 37 °C. Ten microliters of digested PCR product was transformed into chemically competent TOP10 cells. Plasmids from positive transformants were purified and sequenced at the MOBIX facility at McMaster University to confirm the mutation. The mutated *rox* plasmid was transformed into chemically competent BL21 cells for protein expression. Mutated H46Q Rox was expressed and purified as described in section 3.2.2, and activity was tested using the HPLC assay described in section 3.2.7.

3.2.6 Rifamycin MIC determinations

The *rox* gene was subcloned using *Nde*I and *Xho*I into vectors pGDP1 and pGDP2 for minimum inhibitory concentration (MIC) experiments. MICs were determined for various rifamycins according to the CLSI standard broth microdilution method using *E. coli* strain BW25113 *ΔbamB ΔtolC* as the host (61).

3.2.7 Kinetic characterization of Rox by high performance liquid chromatography

Liquid chromatography mass spectrometry (LC/MS) was used to investigate the product of *in vitro* reactions between Rox and several rifamycin substrates. Each reaction contained rifamycin substrate, NADH, Rox enzyme, and was carried out in reaction buffer (50 mM HEPES (pH 7.5), 300 mM NaCl) at room temperature. Reactions were stopped by the addition of an equal volume of cold methanol to precipitate the enzyme and aliquots were spun at 21,000 x g for 3 min. RIF-S and RIF-SV were run on a C8 column, while all other rifamycin substrates were run on a C18 column on an Applied Biosystems QTRAP LC/MS/MS system. Samples were separated using one of two methods, depending on the substrate and column.

For separation on the C8 column, the following method was used:

Total time (min)	Flow rate (µL/min)	Solvent A (%)	Solvent B (%)
0.0	1000	60	40
1.0		60	40
6.0		0	100
8.0		0	100
10.0		60	40
12.0		60	40

where solvent A is water with 0.05% formic acid, and solvent B is acetonitrile with 0.05% formic acid.

For separation on the C18 column, the following method was used:

Total time (min)	Flow rate (µL/min)	Solvent A (%)	Solvent B (%)
0.0	1000	90	10
1.0		90	10
7.0		3	97
8.0		3	97
8.5		90	10
9.0		90	10

where solvent A is water with 0.05% formic acid, and solvent B is acetonitrile with 0.05% formic acid.

Steady state kinetic analysis was determined by a discontinuous reverse phase assay performed using a similar method on a Waters Alliance HPLC system. The K_m values for various rifamycins were determined using the following reaction conditions: 5-100 µM rifamycin substrate, 200 µM NADH, and 3.8 µM Rox. Samples were analyzed for the presence of monooxygenated rifamycin at 5 min. The K_m value for reducing co-substrate NADH and NADPH was determined using the following reaction conditions: 5-1000 µM NAD(P)H, 30 µM RIF-SV, and 0.38 µM Rox. Samples were analyzed for the presence of RIF-SV-O over 5 min.

3.2.8 Purification and structure elucidation of monooxygenated RIF-SV

The reaction of Rox and RIF-SV was scaled up to a volume of 60 mL in a 500 mL flask, containing 12 mg of substrate. The reaction was monitored by LC/MS for complete turnover of

the starting material, taking ~ 2 h. The entire 60 mL reaction was incubated with 3 mL Ni-NTA resin for 30 min at 4 °C before pouring through a column to remove the His-tagged Rox protein. The flow through from the column was frozen and dried by lyophilization. The lyophilized product was crushed and mixed with functionalized C18 resin and poured into a disposable column for purification using a Teledyne Isco CombiFlash chromatography system. Solid phase loading was used to inject the reaction product onto a reverse phase C18 column. The following method was used to separate the product RIF-SV-O from other reaction components:

Total time (min)	Flow rate (mL/min)	Solvent A (%)	Solvent B (%)
0.0	35	100	0
2.4		100	0
2.5		60	40
5.5		60	40
13.6		0	100
15.4		0	100
15.5		20	80
16.9		20	80

where solvent A was water and solvent B was acetonitrile. Fractions were checked by LC/MS for RIF-SV-O and fractions of interest were frozen and lyophilized. The semi-pure CombiFlash fractions were dissolved in less than 1 mL DMSO and purified further by preparative HPLC using an Agilent ZORBAX Eclipse XDB-C8 column (4.6 x 150 mm; 5 µm) and the following gradient:

Total time (min)	Flow rate (µL/min)	Solvent A (%)	Solvent B (%)
0.0	1000	55	45
1.0		55	45
6.0		0	100
8.0		0	100
10.0		55	45
12.0		55	45

where solvent A was water with 0.05% formic acid and solvent B was acetonitrile with 0.05% formic acid. Fractions from HPLC were collected on ice, pooled and flash frozen immediately after eluting. The pooled HPLC fractions were lyophilized and re-dissolved in 50:50 water: acetonitrile before transferring to a pre-weighed vial and lyophilizing again. The final product was dissolved in deuterated DMSO and submitted for 1D and 2D NMR experiments on a Bruker AVIII 700 MHz instrument equipped with a cryoprobe. NMR analysis was performed by Dr. Kalinka Koteva in the Wright lab. High resolution mass and tandem mass spectrometry data was obtained using an Agilent 1260 Infinity liquid chromatography system attached to a 6550 QTOF mass spectrometer in negative mode.

3.2.9 Investigating the Rox reaction under anaerobic and $^{18}O_2$ conditions

To investigate the Rox reaction under anaerobic conditions, a flask containing 1 mM RIF-SV and 20 mM NADH in 8 mL of reaction buffer was degassed under vacuum for 5 min. Nitrogen gas was then bubbled into the solution, which was kept under vacuum for another 5 min. Buffer containing Rox was added to bring the reaction volume up to 15 mL and this was bubbled with nitrogen and degassed again. This was left under nitrogen for 15 min before opening the flask to remove an aliquot for analysis by HPLC. To investigate the Rox reaction under $^{18}O_2$ conditions, a flask containing 50 mg RIF-SV and 2 mM NADH in 25 mL reaction buffer was degassed under vacuum for 5 min. Nitrogen gas was then bubbled into the solution, which was kept under vacuum for another 5 min. Buffer containing Rox was added to bring the volume up to 50 mL and this was bubbled with nitrogen and degassed again. $^{18}O_2$ gas was then bubbled into the solution in the flask and left to sit, swirling occasionally, for 1 h. After one h the flask was opened to remove an aliquot for LC/MS analysis. The reaction product, RIF-SV-^{18}O, was purified as described in section 3.2.7.

3.2.10 Assessing the antibiotic activity of RIF-SV-O

A disk assay was performed to observed whether RIF-SV-O retained antibiotic activity. A lawn of *E. coli* BW25113 *ΔbamB ΔtolC* was swabbed onto an agar plate. 10 µL of RIF-SV and RIF-SV-^{18}O were spotted on paper disks on an agar plate. 5 µL of ampicillin was spotted as a positive control, and 10 µL of 20% DMSO was spotted as a vehicle control. The plate was incubated at 37 °C for 20 h before observing.

3.3 Results

3.3.1 Degradation of rifamycins by S. venezuelae

To test whether *S. venezuelae* was capable of degrading rifamycins, cultures of *S. venezuelae* were grown in the presence of low levels of either RIF or RIF-SV and monitored over two days. Aliquots were taken at 12, 24, 36, and 48 h after the addition of rifampin and run on the LC/MS for analysis. The result for RIF is shown; the same trend was observed for RIF-SV. As seen in Figure 3.3, rifampin disappears over 48 h. Both peaks on the chromatogram are RIF; this is a result of the quinone-hydroquinone system on the aromatic core of the rifamycin scaffold. One is the quinone form (oxidized) and the other is the hydroquinone (reduced). This is consistent with the previous observations that the presence of a rifampin monooxygenase gene causes decomposition of RIF.

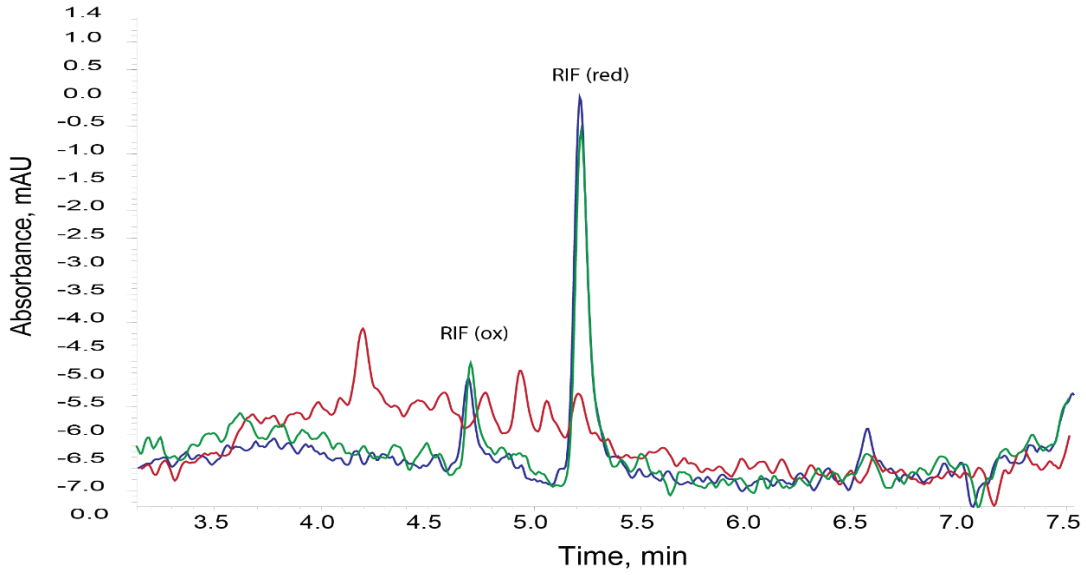

Figure 3.3 Chromatogram from *S. venezuelae* cultured with RIF, extracted at 300 nm. The blue trace represents 24 h after RIF addition, the red represents 72 h after RIF addition, and the green represents a control of media plus RIF after 72 h. The two peaks represent the two forms of RIF: the oxidized quinone (RIF(ox)) and the reduced hydroquinone (RIF(red)).

3.3.2 Cloning, expression and purification of Rox

Purified His-tagged Rox was run on an SDS-PAGE gel to confirm the size of the protein. A band consistent with the predicted molecular weight of 52 kDa was observed and is shown in Figure 3.4. The molecular weight of native Rox protein was also confirmed by analytical gel filtration (section 3.2.3). The purified Rox enzyme was bright yellow in colour, as expected by the prediction of a bound flavin cofactor. The UV-Vis spectrum of Rox was measured, and is shown in Figure 3.5. The visible spectrum contains absorbance maxima at 370 nm and 450 nm as well, which are characteristic of FAD.

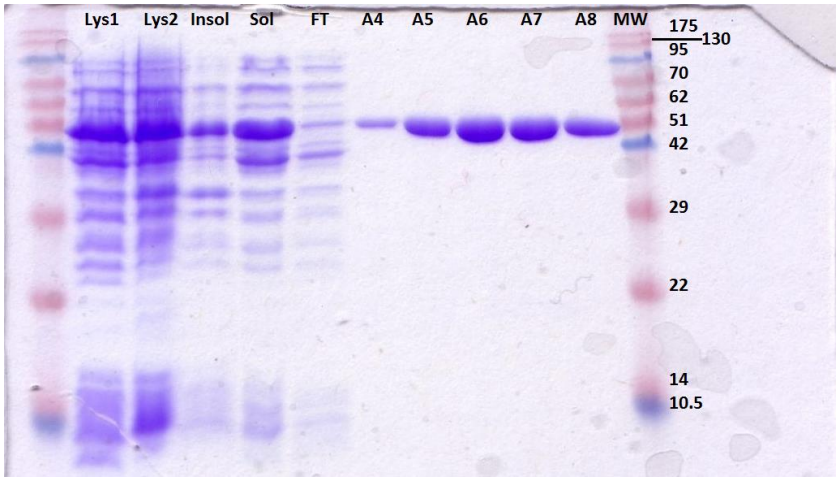

Figure 3.4 Overexpression and purification of Rox. Lys1= cell lysate 1st passage; Lys2= cell lysate 2nd passage; Insol= insoluble pellet; Sol= clarified supernatant (soluble); FT= flow through. A4-A8 are FPLC collected fractions containing Rox, which has an approximate molecular weight of 52 kDa.

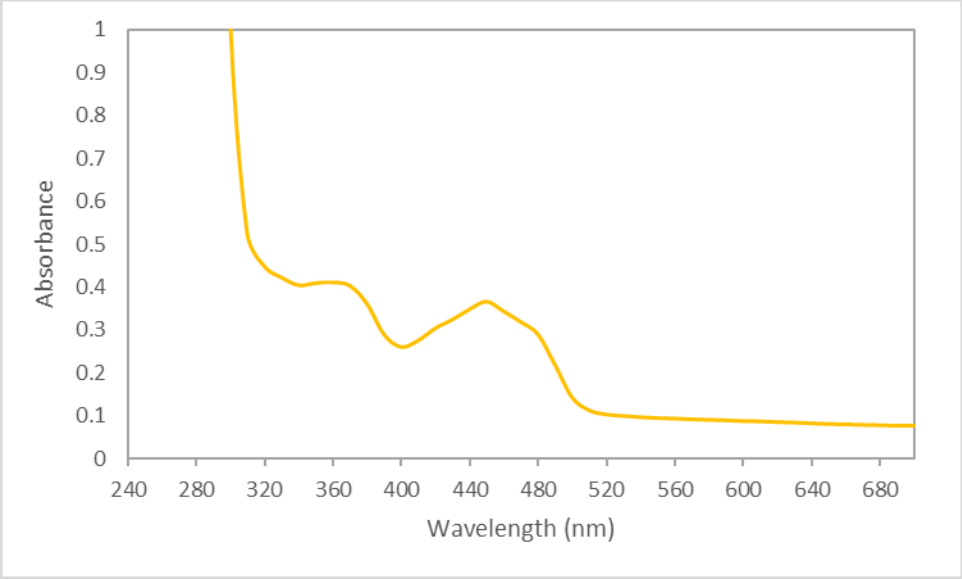

Figure 3.5 UV-Vis absorbance spectrum of Rox, containing the characteristic absorbance maxima at 370 and 450 nm, indicative of a bound FAD cofactor.

3.3.3 Cleavage of the His-tag and infusion with the substrate for crystallography

For protein crystallography, we removed the His-tag that was used to initially purify Rox. The protein was then concentrated and purified further using an analytical gel filtration column. This column was calibrated using a gel filtration LMW kit according to the manufacturers guidelines, allowing for the determination of protein size. From this column, Rox eluted as a single peak with the approximate size of 50 kDa, agreeing with the SDS-PAGE analysis. This indicates that Rox is a monomeric protein. For co-crystallization with the substrate rifampin, the drug was infused into the protein before setting trays. This resulted in the protein solution changing colour from the native yellow to orange, as seen in Figure 3.6.

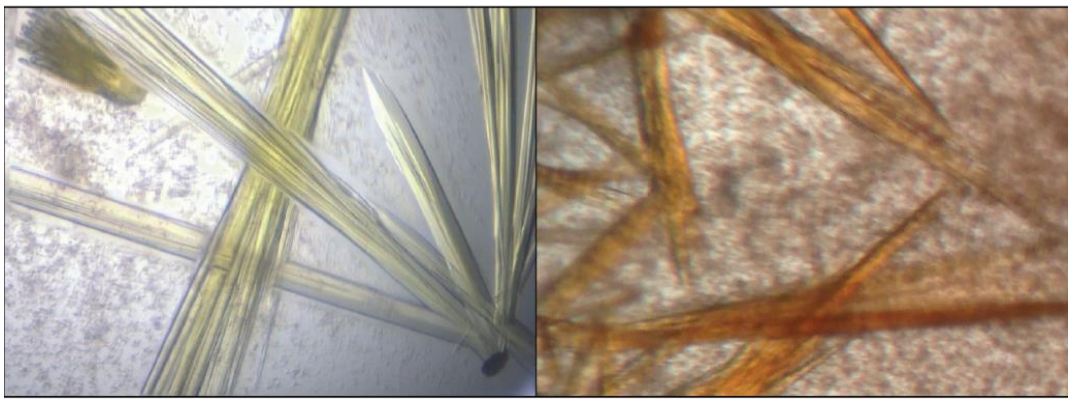

Figure 3.6 Crystals of Rox. On the left, apo-Rox is yellow in colour due to the FAD cofactor. On the right, bound RIF causes the protein to become orange-red.

3.3.4 The crystal structure of Rox

Initial conditions for protein crystallography were screened using the commercially available kits from Qiagen. Of the 192 conditions screened, seven had crystal growth. These conditions are listed in Table 3.1. Each condition was then systematically screened by tuning the pH and PEG concentration to find conditions optimal for crystal growth. Fine screening was performed using hanging drop trays, and crystals grew within 24 h both in the presence and absence of RIF. Crystals of apo-Rox and Rox with RIF were grown in 0.1 M MES (pH 6), 25% PEGm 5k, 0.2 M $(NH_4)_2SO_4$. Data collection took place at McMaster and data was analyzed by Dr. Georgina Cox in the Wright lab. Both apo- and RIF bound Rox crystallized with 3 molecules in the asymmetric unit.

To find the closest structural analogs of Rox, the protein sequence was submitted to the I-TASSER server (70). This returned the monooxygenases PgaE and CabE, involved in angucycline biosynthesis, OxyS involved in oxytetracycline biosynthesis, and MtmOIV, involved in mithramycin biosynthesis (66,71,72). Their structures are shown in Appendix 2.

Table 3.1 Crystallography conditions producing hits in the initial screen of Classics and Classics II (Qiagen).

H8 – Classics 0.1M MES pH 6.5 30% PEGm 5k 0.2M $(NH_4)_2SO_4$	H3 – Classics 0.1M $Na_3(C_6H_5O_7)$ pH 5.6 30% PEG 4k 0.2M $NH_4(CH_3CO_2)$	G2 – Classics 0.1M BIS TRIS pH 6.5 25% PEG 3.35k Li_2 SO_4	F10 – Classics 0.1M $Na(CH_3)_2AsO_2$ pH 6.5 30% PEG 8k 0.2M $(NH_4)_2SO_4$
F8 – Classics 0.1M $Na(CH_3)_2AsO_2$ pH 6.5 20% PEG 8k 0.2M $Mg(CH_3CO_2)_2$	F7 – Classics 0.1M $Na(CH_3)_2AsO_2$ pH 6.5 18% PEG 8k 0.2M $Ca(CH_3CO_2)_2$	D10 – Classics II 0.1M BIS TRIS pH 6.5 20% PEGm 5k	

A multiple sequence alignment of these proteins was performed and is shown in Figure 3.7. These proteins share approximately 50% identity. A model for molecular replacement was built by Phenix.ensembler using the PDB structures of these enzymes and the multiple sequence alignment. The structure of Rox was solved by molecular replacement using this model. The structure without RIF is currently refined to 2.9 Å, while the structure with RIF has not been refined from the molecular replacement model at this time. The more refined apo-structure is shown in Figure 3.8. Some disordered regions of the enzyme could not be modeled in; specifically, the loop between 181-220, which has been observed to be disordered in the other monooxygenases as well (65,66,72).

Similar to other monooxygenases, Rox has three domains: the FAD binding domain (1-163, 259-380), the middle domain (164-258), and the C-terminal domain (381-476). The FAD binding domain is responsible for binding both FAD and reducing cofactor, as well as forming part of the substrate binding pocket. It is in this domain where most of the identity among monooxygenases occurs, as illustrated in Figure 3.9. The middle domain is inserted in the FAD binding domain in the primary sequence. Consistent with the other monooxygenase structures,

there is a large disordered loop in this region; in Rox this corresponds to residues 181- 220. This domain forms the roof of the substrate binding pocket. There is a lot of variability in this domain between structures.

The binding pocket for RIF can be seen in Figure 3.10. It is mostly hydrophobic which is consistent with other proteins that bind RIF, due to the hydrophobicity of the molecule. The aromatic core if the RIF molecule is pointing in towards the FAD binding pocket, while the semisynthetic tail at C3 points out (Figure 3.11). This suggests that the tail may not be the site of monooxygenation, as was previously believed.

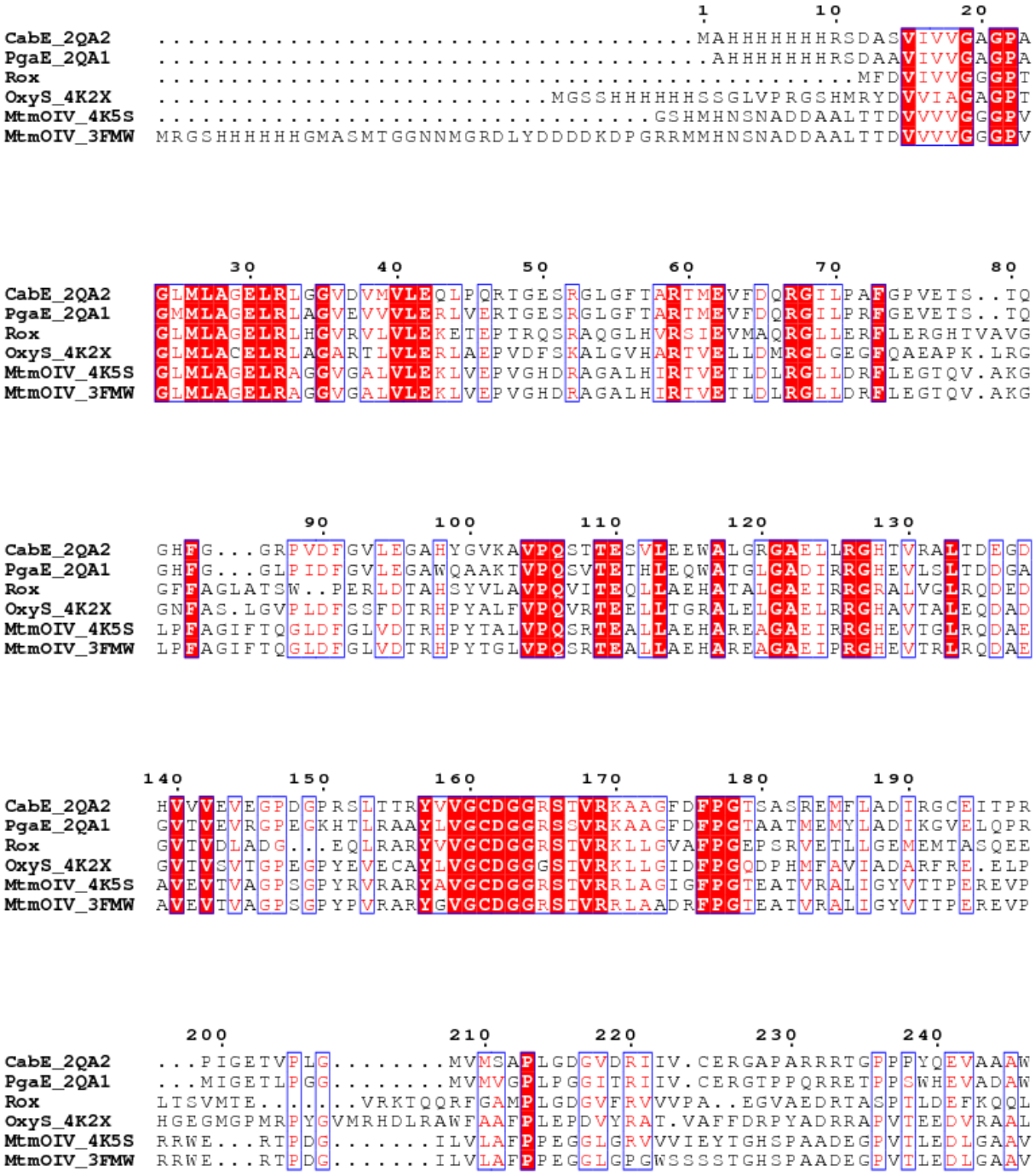
CabE_2QA2
PgaE_2QA1
Rox
OxyS_4K2X
MtmOIV_4K5S
MtmOIV_3FMW

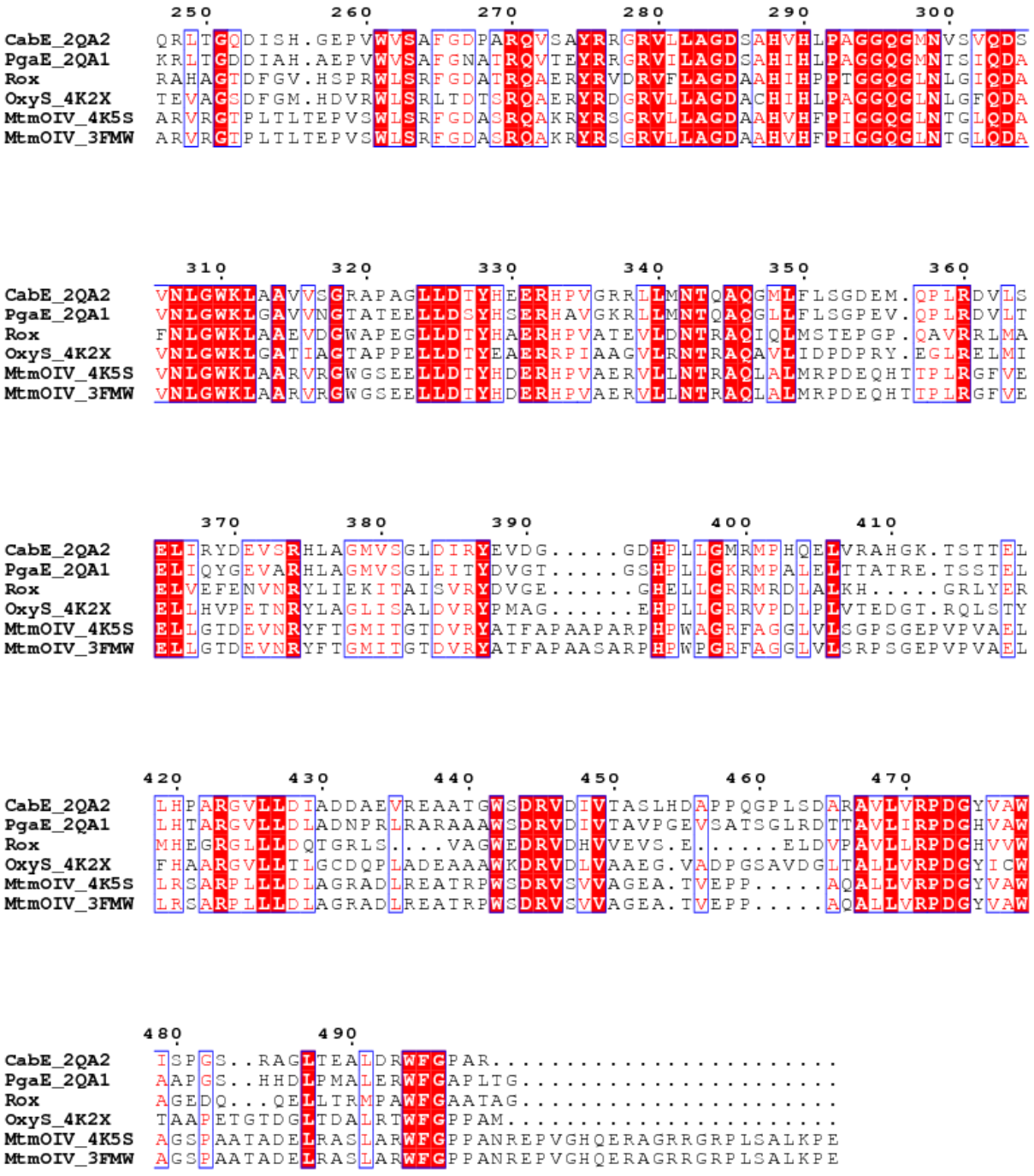

Figure 3.7 Multiple sequence alignment of monooxygenases most similar to Rox, as identified by I-TASSER. The name of the enzyme and its PDB code are labelled at the left. Residues with white text in red columns are identical; residues with red text with blue columns are similar.

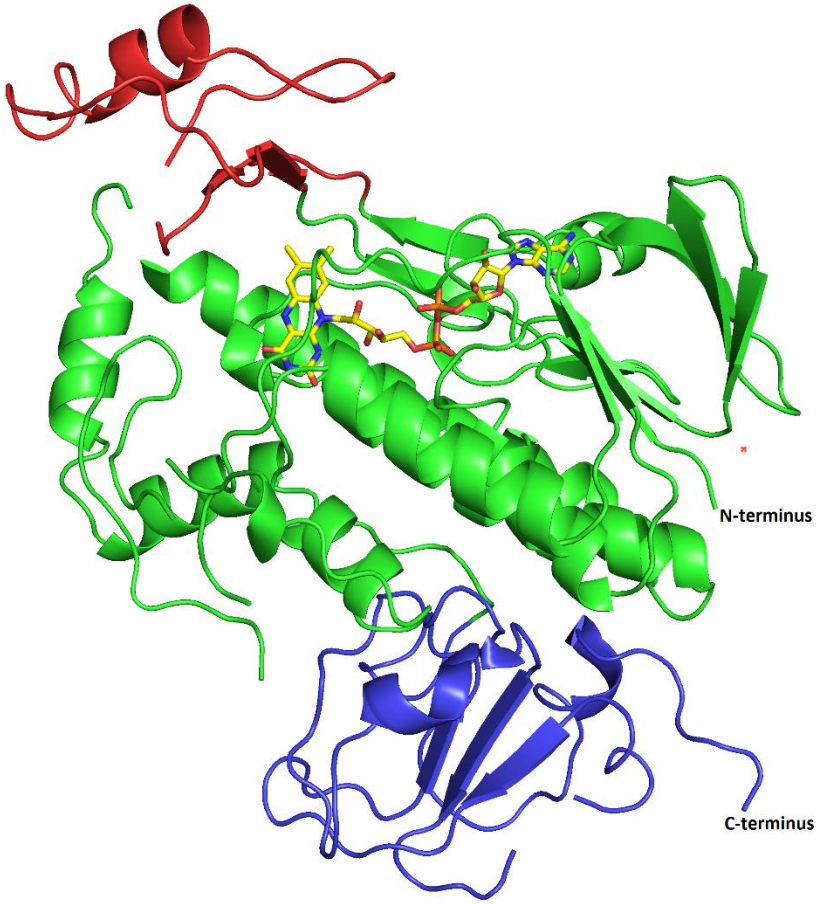

Figure 3.8 The apo-Rox crystal structure, partially refined to 2.9 Å. The three domains are colour coded: FAD binding (green), middle (red) and C-terminal (blue). The FAD cofactor is shown. Parts of the structure are missing; this is due to some disordered regions in the structure that could not be modeled in.

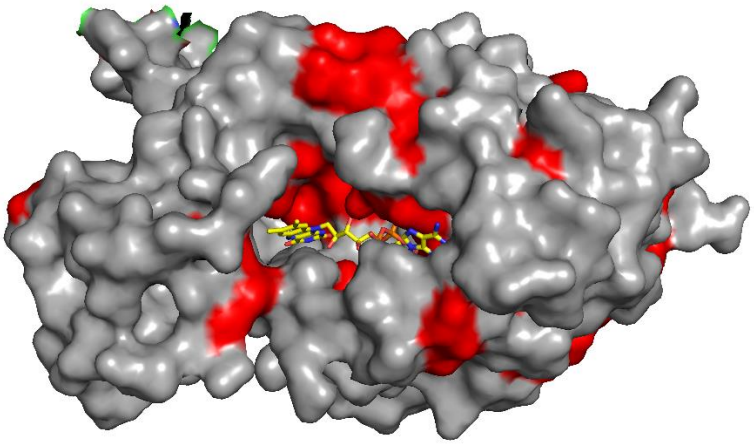

Figure 3.9 The FAD binding pocket of Rox. The red represents identity among monooxygenases identified as closest structural analogs to Rox by I-TASSER. The FAD molecule is shown.

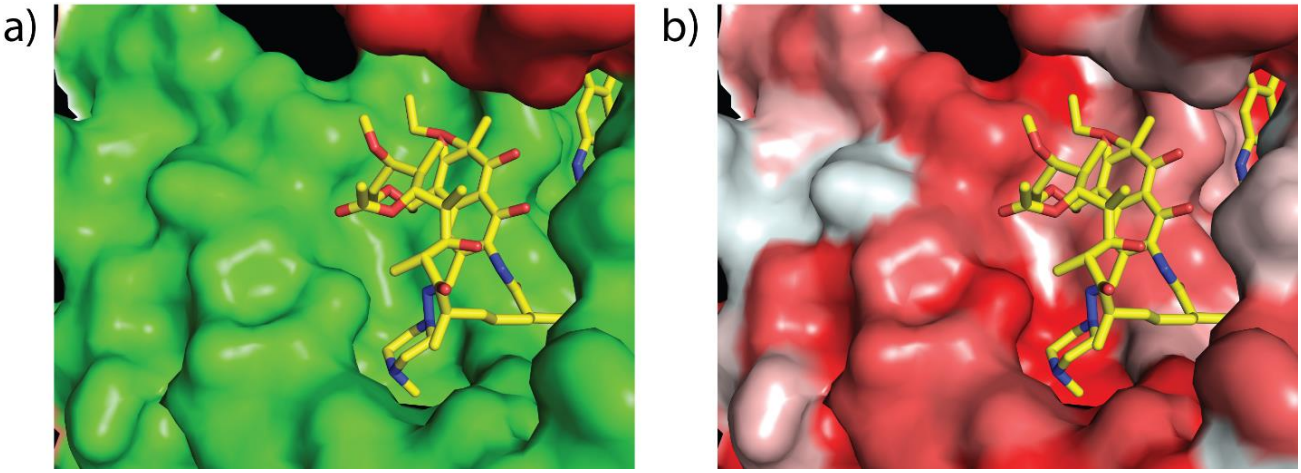

Figure 3.10 The RIF binding pocket of Rox. a) The domains are coloured in the same way as Figure 3.8: the FAD binding domain in green and the middle domain in red, showing how these two domains form the binding pocket. b) The colouring represents hydrophobicity: red is most hydrophobic and white is least hydrophobic, showing the hydrophobicity of the RIF binding pocket.

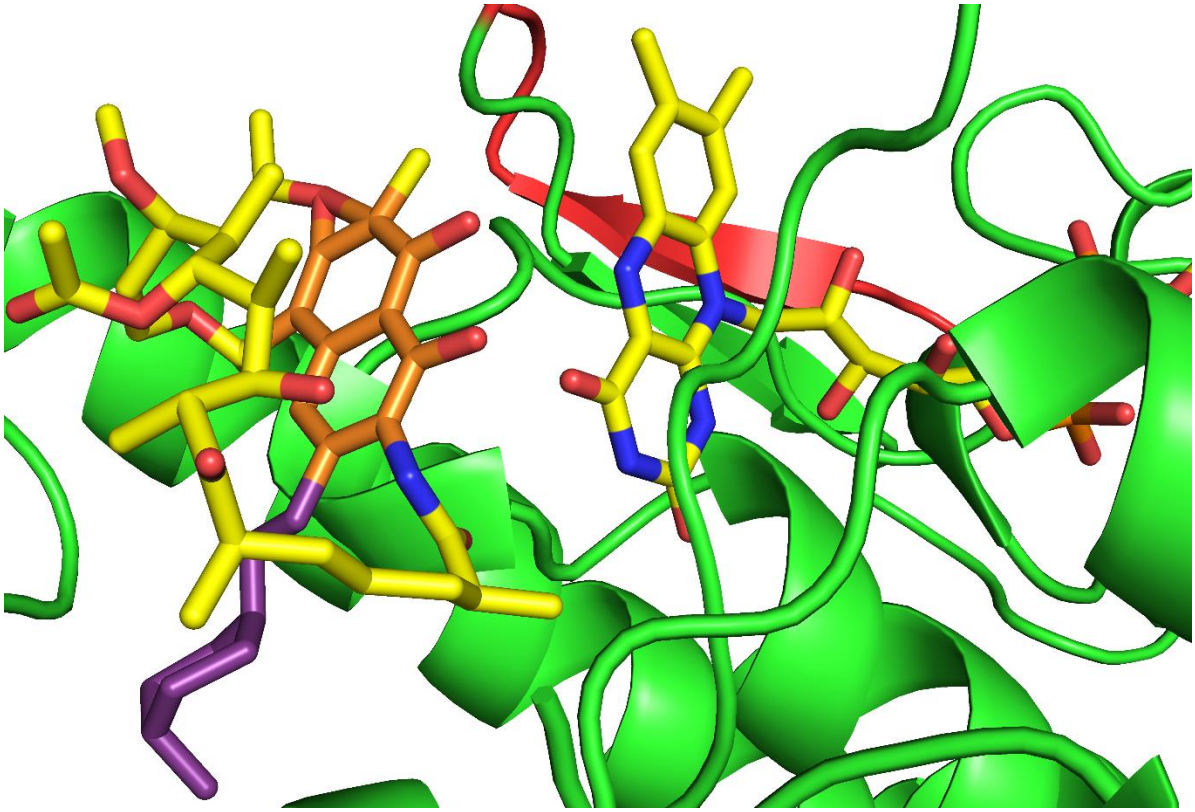

Figure 3.11 Orientation of RIF and FAD bound to Rox. This image was generated from the unrefined model of Rox with RIF. The aromatic core of RIF is coloured orange, while the semisynthetic tail on C3 is coloured purple.

The C-terminal domain is not known to be involved in the enzymatic reaction. A C-terminal domain truncation of PgaE was not expressed, indicating that this part of the enzyme may be involved in folding stability. We are in the process of generating a C-terminal truncation to test whether this is the same for Rox.

3.3.5 Rox confers resistance to rifamycins

To examine whether Rox was conferring resistance to rifamycins, we tested the minimum inhibitory concentration (MIC) of various rifamycins towards *E. coli* with and without the *rox* gene. The *E. coli* strain used, BW25113 *ΔbamB ΔtolC,* was constructed in the Wright lab and is hypersensitive to drugs due to the deletion of *bamB* (involved in membrane permeability) and *tolC* (involved in efflux). We used this strain since rifamycins generally have poor activity against Gram-negative bacteria like *E. coli* due to poor permeability. The pGDP1 and 2 vectors were also constructed in the Wright lab, and are part of a tunable platform for expressing antibiotic resistance genes. The *rox* gene was cloned under a strong (pGDP1) and weak (pGDP2) promoter and transformed into *E. coli* BW25113 *ΔbamB ΔtolC* for MIC determination. The results are summarized in Table 3.2. Normally a higher MIC would be observed for the resistance gene under control of the strong promoter, however here both promoters give relatively similar MIC values. The presence of the *rox* gene confers at least 5-fold resistance to all rifamycins tested except rifabutin (RIFAB). This highlights the ability of Rox to confer resistance to not only natural products but additionally to clinically relevant rifamycin antibiotics.

Table 3.2 Rifamycin MIC determinations of *rox* heterologously expressed in *E. coli* strain BW25113 ΔbamB ΔtolC

Rifamycin	MIC (μg/mL)		
	No construct	pGDP2-*rox*	pGDP1-*rox*
RIF-SV	2	≥256	≥256
RIF-S	≤0.5	≥256	≥256
RIF	1	128	64
RIFAP	≤0.5	16-32	16
RIFAX	≤0.5	16-32	16
RIFAB	≤0.5	1-2	1

3.3.6 Confirming Rox activity in vitro using an LC/MS assay

To test the activity of the purified Rox, an *in vitro* assay was developed. This reaction contained the rifamycin substrate, the enzyme, buffer, and a reducing co-substrate NADH. Like other flavin dependant monooxygenases, a reducing co-substrate was required; in the absence of this co-substrate the reaction did not occur. LC/MS was used to confirm the activity of the enzyme. Figure 3.12 shows the LC/MS analysis of the reaction with RIF-SV as the substrate. Both the original starting material RIF-SV (696.36) and RIF-S (694.62) are present; this is due to the non-enzymatic conversion of RIF-SV to RIF-S in aqueous, aerated solutions (73). The predicted molecular weight of monooxygenated RIF-SV is 713.3047 Da. Interestingly, two products were formed: in negative mode their masses are 712.32 and 714.54 Da. The 712.32 mass product represents the $[M-H]^-$ ion for the monooxygenated RIF-SV (RIF-SV-O). The second product could be the $[M-H]^-$ ion for a reduced form of RIF-SV-O, or RIF-SV-O +2H. This trend of two reaction products was observed for other rifamycin substrates, as seen in Table 3.3. It should be noted that very little product was formed for rifabutin; this is consistent with the very modest increase in MIC for this substrate. Using this *in vitro* assay, kinetic parameters for Rox were assessed using a discontinuous, reverse phase HPLC assay.

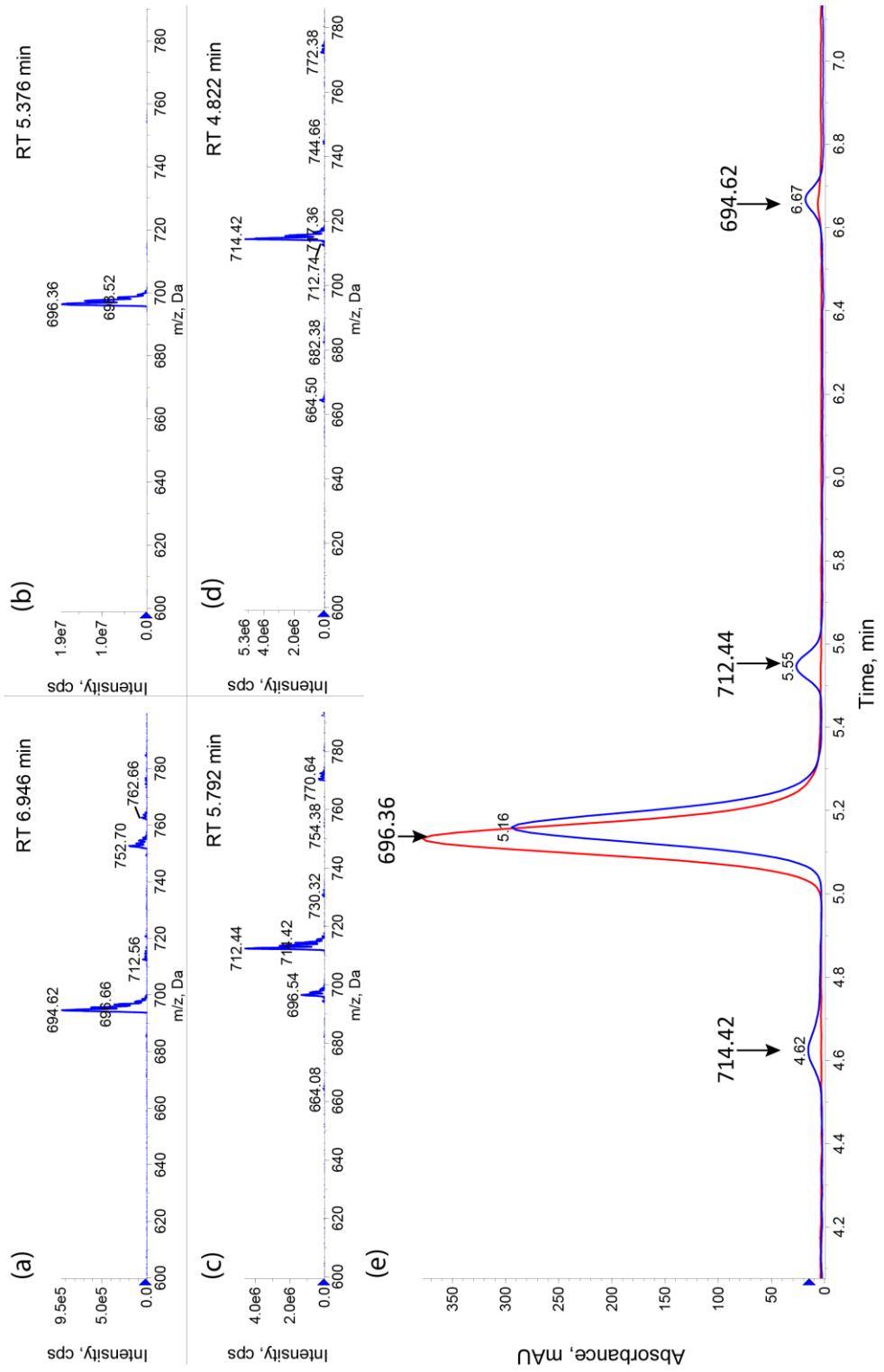

Figure 3.12 LC/MS analysis of the reaction with RIF-SV. Panel (e) shows the chromatograms of reactions with (blue) and without (red) enzyme. The 4 peaks represent the 4 species present: the two starting materials RIF-SV (696.36) and RIF-S (694.62), and two products with masses of 712.44 and 714.42. Panels (a) - (d) show the mass spectra of each peak. RT represents the retention time of each peak.

Table 3.3 LC/MS analysis of *in vitro* reactions with various rifamycin substrates

Rifamycin	Predicted mass of monooxygenated product (Da)	Observed mass ($[M-H]^-$) of "Product 1"	Observed mass ($[M-H]^-$) of "Product 2"
RIF-SV	713.3047	712.32	714.54
RIF	837.3928	837.60	839.76
RIFAP	891.4397	891.48	893.40
RIFAX	800.3400	800.40	802.44
RIFAB	861.4291	861.48	863.64

3.3.7 Discontinuous, reverse phase HPLC assay of Rox steady-state kinetics

Reactions were set up with varying concentrations of rifamycin substrate, NADH, and Rox to optimize the HPLC assay. Aliquots were taken at fixed time points and quenched with cold methanol, before separating on a reverse phase chromatography column. Figure 3.13 shows an example of the reaction progress monitored at 400 nm. The product peaks were integrated and area under the curve was plotted against time to generate progress curves. From these, the reaction was found to be linear over 5 min, and this time scale was used for steady state kinetic assays. One substrate concentration ranged from 5-200 µM while the other was held in excess to determine kinetic parameters for both rifamycins and reducing co-substrates. The GraFit software was used to fit data to Michaelis-Menten curves, as seen in Figure 3.14 and Figure 3.15. Table 3.4 lists kinetic constants for Rox. As expected from the colorimetric observation of the reactions, RIF-SV is the best substrate. As well, the enzyme can use either NADH or NADPH as a co-substrate, however NADH is preferred.

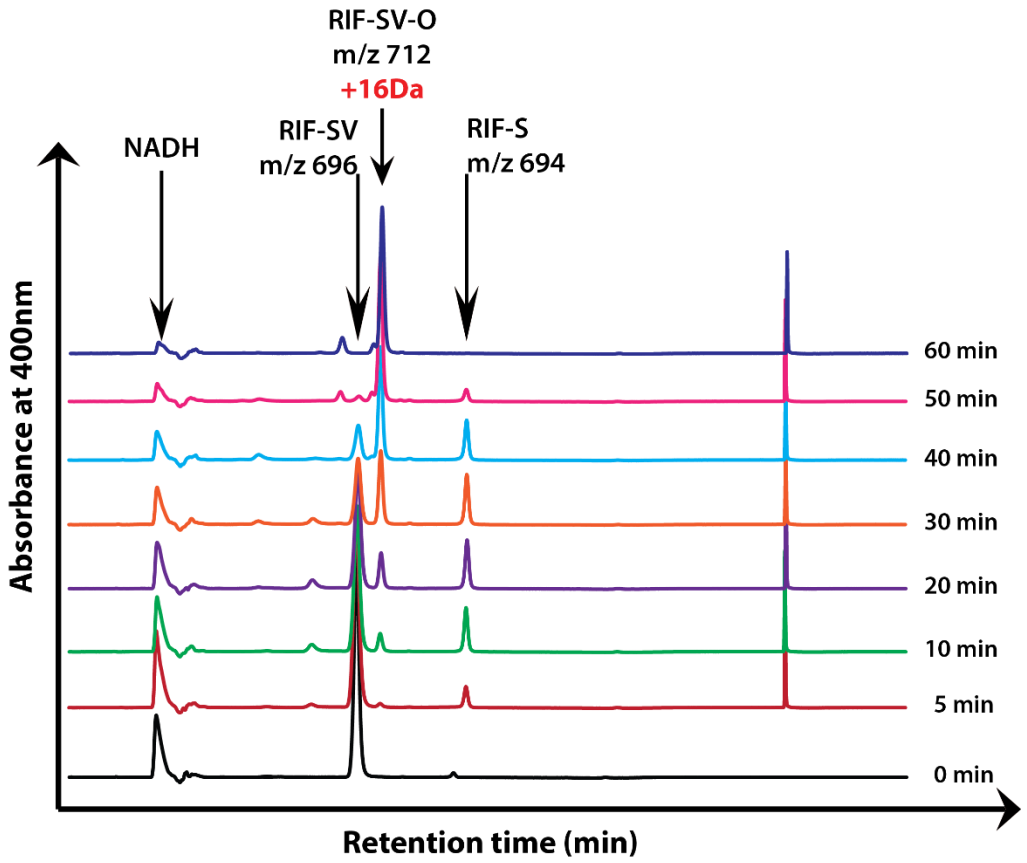

Figure 3.13 HPLC chromatograms showing progression of the reaction over time. The black chromatogram at 0 min is prior to the addition of Rox; the following coloured chromatograms represent 5- 60 min, in which the starting material RIF-SV is completely converted to the product RIF-SV-O.

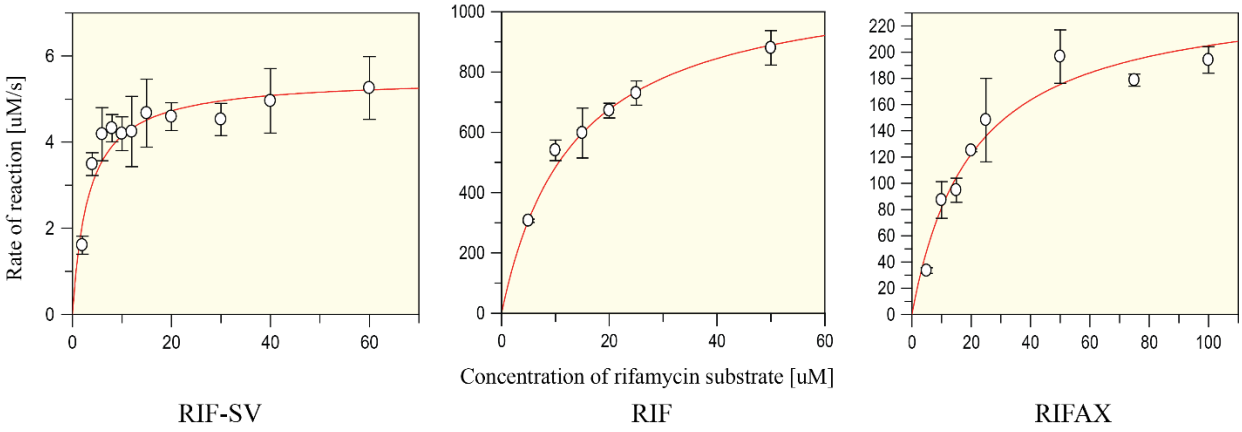

Figure 3.14 Michaelis-Menten curves for Rox with rifamycin substrates tested: RIF-SV, RIF, and RIFAX. Each concentration was repeated in triplicate. NADH concentration was held at 200 µM.

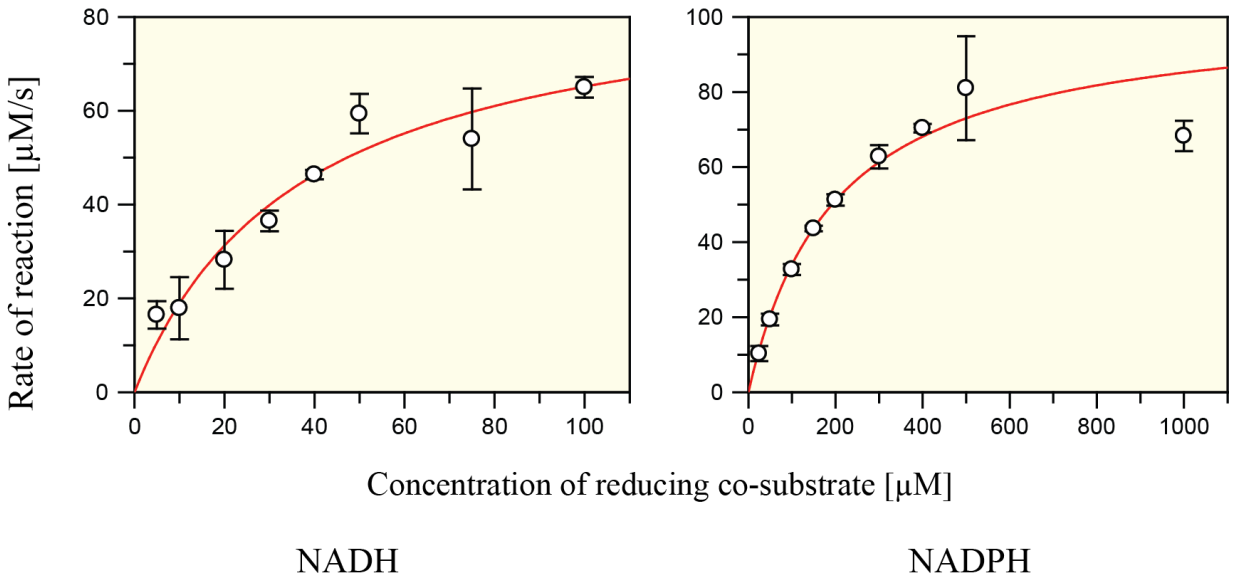

Figure 3.15 Michaelis-Menten curves for Rox with reducing co-substrates tested: NADH and NADPH. Each concentration was repeated in triplicate. RIF-SV concentration was held at 30 µM.

Table 3.4 Steady-state kinetic parameters of Rox

Substrate	K_m (µM)	V_{max} (µM/s)	[Rox] (mg/mL)	Total Enzyme (µM)	k_{cat} (1/s)	k_{cat}/K_m ($\mu M^{-1}s^{-1}$)
RIF-SV	3.27	5.49	0.01	0.19	28.79	8.81
RIF	13.24	1124.08	0.20	3.82	294.51	22.24
RIFAX	20.39	246.8470	0.20	3.82	64.67	3.17
NADH	37.20	89.40	0.02	0.38	234.22	6.30
NADPH	200.44	102.26	0.02	0.38	267.92	1.34

3.3.8 Structure elucidation of monooxygenated RIF-SV

The structure of monooxygenated rifampin was previously proposed, with the modification occurring on the tail region of the molecule. For this reason, we were intrigued to see that RIF-SV was a substrate for Rox, since it lacks a tail region. We decided to purify monooxygenated RIF-SV for structure elucidation. The Rox reaction was scaled up to contain 12 mg of RIF-SV; this scaled up reaction was performed in triplicate. The product RIF-SV-O was

purified by chromatography as described in section 3.2.8. The UV-Vis spectra of RIF-SV-O differs significantly from that of RIF-SV; it is more consistent with the spectra of RIF-S (Figure 3.16). The purified RIF-SV-O was dissolved in deuterated DMSO and submitted for 1D and 2D NMR analysis. Chemical shifts are reported in ppm relative to tetramethylsilane (TMS), using the residual solvent signals at 2.50 and 39.50 ppm as internal standards for H^1 and C^{13} respectively (Appendix 3). The chemical shifts were compared to those of RIF-SV and RIF-S. Knowing that Rox is a flavin dependent monooxygenase, we hypothesized that Rox may hydroxylate RIF-SV on the aromatic core of the molecule. However, all protons in the RIF-SV spectrum are accounted for in the RIF-SV-O spectrum, ruling out C3 as the site of monooxygenation via a hydroxylase type mechanism. One interesting phenomenon observed in the ^{15}N heteronuclear single-bond correlation (HSQC-^{15}N) experiment was the presence of two protons bound to the only nitrogen atom in the rifamycin scaffold, as seen in Figure 3.17. This suggested a ring opening event taking place. With that in mind, the structure of RIF-SV-O was solved by Dr. Kalinka Koteva in the Wright lab, illustrated in Figure 3.18. Note that the hydroxylation is proposed to occur on C2; this is in part due to the hypothesized mechanism, which will be discussed in section 3.4.

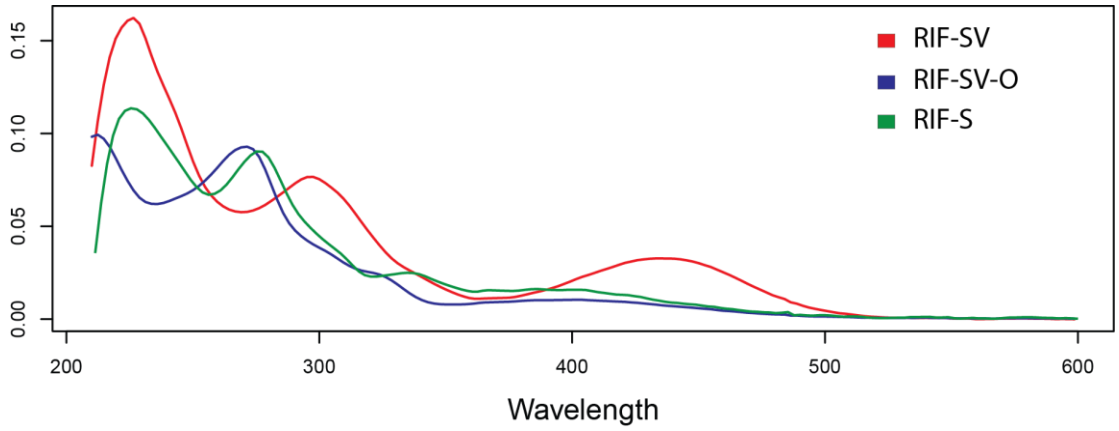

Figure 3.16 Comparison of the UV-Vis spectra of RIF-SV, RIF-S, and RIF-SV-O

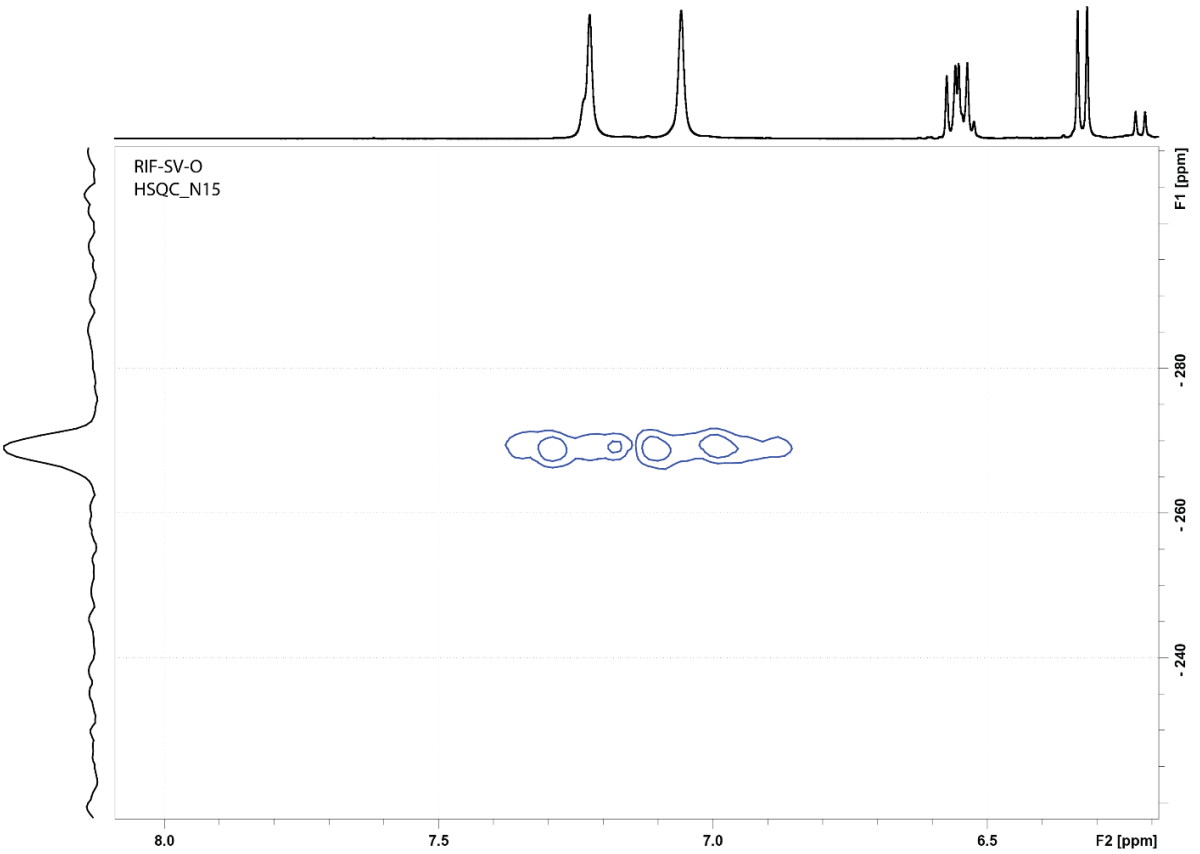

Figure 3.17 HSQC-^{15}N 2D NMR spectra. Along the top is the proton spectra and along the left is the nitrogen spectra. Dots on the 2D spectra represent protons directly bound to a nitrogen atom. Clearly both protons are bound to the nitrogen atom.

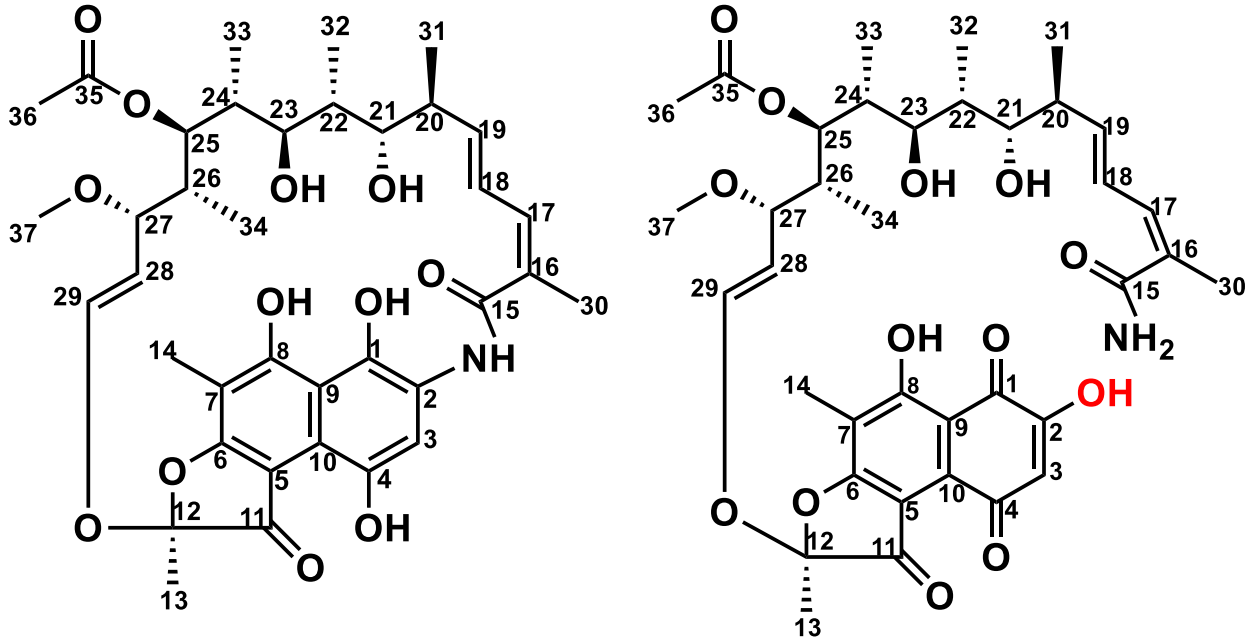

Figure 3.18 Structure of RIF-SV-O. The oxygen added by Rox is highlighted in red.

3.3.9 High resolution MS/MS analysis of monooxygenated rifamycins

To confirm our hypothesis that ring cleavage and C2 hydroxylation occurs, we performed tandem mass spectrometry analysis of RIF-SV-O and other monooxygenated rifamycins. Reactions were prepared with 300 µM rifamycin substrate, 1 mM NADH, and 1 mg/mL Rox. Aliquots were taken after 30 min, quenched with methanol, and diluted by a factor of 10. Stocks of rifamycin substrates were diluted to 30 µM. Samples were run on the high resolution LC/MS instrument in negative mode to obtain high resolution masses for both the starting material and product of the reaction. These data are summarized in Table 3.5. All of the substrates tested showed some product formation *in vitro* and the expected and observed masses are very close. Substrate and product ions were then fragmented in negative mode and compared.

The aromatic core fragment of rifamycins is easily identified in MS/MS experiments (74,75), and these core fragments were compared between starting material and product, as seen in Table 3.6. The masses of the core fragments are very similar between the starting material and product, as illustrated in Table 3.6. If we consider the structures in Figure 3.19, the hydroxylation at C2 replaces the amine group normally present at this position, and the mass of the core fragment remains nearly the same. Indeed, the fragmentation data seems to support this hypothesis, as indicated by the low error values. In contrast, note the incredibly high error for the rifapentine product from Table 3.6. The mass of the observed product is 1.0079 Da larger than expected; this suggests that the aromatic core fragment of rifapentine is actually protonated, in which case the error reduces to 0.22 ppm. Also of note is that the product ion for rifabutin could not be fragmented, due to its low abundance.

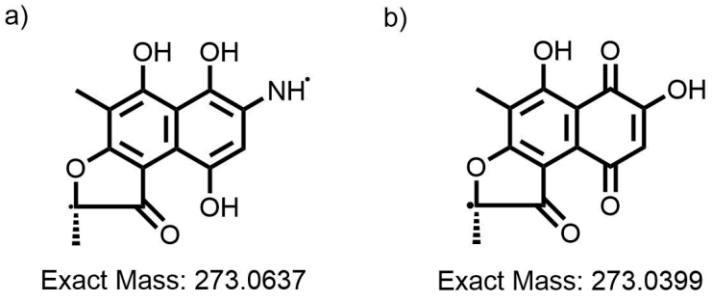

Figure 3.19 Structures of the aromatic core fragments of a) RIF-SV and b) RIF-SV-O. Note that the masses are very similar despite the structural differences.

Table 3.5 High resolution mass data for rifamycin starting materials and products

Rifamycin	Expected *m/z* starting material	Observed *m/z* starting material	Error (ppm)	Expected *m/z* monooxygenated product	Observed *m/z* monooxygenated product	Error (ppm)
RIF-SV	696.3025	696.3082	8.19	712.2975	712.2984	1.26
Rifampin	821.3978	821.3997	2.31	837.3928	837.3927	-0.12
Rifapentine	875.4448	875.4509	6.97	891.4397	891.4397	0.00
Rifabutin	845.4342	845.4377	4.14	861.4291	861.4285	-0.70
Rifaximin	784.3451	784.3468	2.17	800.34	800.3399	-0.12

Table 3.6 Comparison of aromatic core fragment mass for rifamycin starting materials and products

Rifamycin	Expected *m/z* for aromatic core fragment starting material	Observed *m/z* for aromatic core fragment starting material	Error (ppm)	Expected *m/z* for aromatic core fragment product	Observed *m/z* for aromatic core fragment product	Error (ppm)
RIF-SV	272.0564	272.0568	1.47	272.0326	272.0321	-1.84
Rifampin	397.1517	397.1519	0.50	397.1279	397.1273	-1.51
Rifapentine	451.1987	451.1986	-0.22	451.1749	452.1828	2233.95
Rifabutin	421.1881	421.1867	-3.32	421.1643	-	-
Rifaximin	360.099	360.0979	-3.05	360.0752	360.0754	0.56

3.3.10 Investigating the Rox reaction under anaerobic and $^{18}O_2$ conditions

Rox is a flavin dependant monooxygenase and we hypothesized that it is mechanistically similar to other flavin dependant monooxygenases which use molecular oxygen as the oxygen source for hydroxylation. To confirm this, we investigated the reaction under anaerobic conditions, with our hypothesis being that no reaction would occur. No product formation was observed under anaerobic conditions. We also decided to perform the reaction under $^{18}O_2$ labelled gas to observe whether incorporation of the heavy oxygen would occur. This reaction was performed as described in section 3.2.9 of this thesis. Table 3.7 shows high resolution mass analysis of the aliquot taken from the $^{18}O_2$ labelling reaction. The mass of both the product and the aromatic core fragment of the molecule increases by 2 Da as expected, confirming that molecular oxygen is the oxygen source. The RIF-SV-^{18}O was purified in the same manner as RIF-SV-O, described in section 3.2.8 of this thesis.

Table 3.7 High resolution mass spectrometry analysis of RIF-SV-^{18}O

	Expected mass of monooxygenated product	Observed mass of monooxygenated product	Error (ppm)	Expected mass of product aromatic core fragment	Observed mass of product aromatic core fragment	Error (ppm)
RIF-SV-^{18}O	714.3017	714.3010	-0.98	274.0369	274.0369	0.00

3.3.11 Testing the antibiotic activity of RIF-SV-O

To determine whether the RIF-SV-O product had antibiotic activity, we performed a disk diffusion assay against *E. coli* strain BW25113 *ΔbamB ΔtolC*. Onto a lawn of this *E. coli* strain, disks containing RIF-SV, RIF-SV-^{18}O, ampicillin, and 20% DMSO were placed. The ampicillin

was a positive control, while the 20% DMSO was a negative control. RIF-SV-^{18}O was used as it was the most recently purified RIF-SV-O product and available at the time. Equal concentrations in milligrams per millilitre were used for RIF-SV and RIF-SV-O. Figure 3.20 shows the result. RIF-SV-O shows no zone of inhibition; however, when a higher concentration of product was tested, small zones were observed. RIF-SV-O then has significantly less activity than RIF-SV

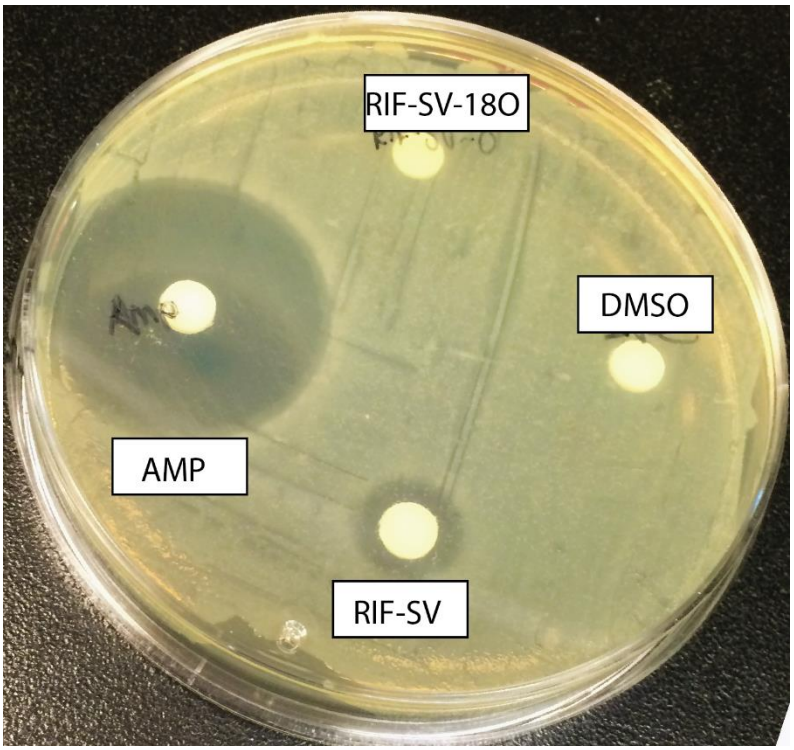

Figure 3.20 Disk diffusion assay to test for antibiotic activity of RIF-SV-O. Clockwise starting from the top: RIF-SV-^{18}O, 20% DMSO, RIF-SV, and ampicillin (AMP).

3.4 Discussion

The environment has been shown to be a vast reservoir for antibiotic resistance genes (76). The *rox* gene was identified as being responsible for the decolourization and subsequent decomposition of rifamycins from an environmental opportunistic pathogen (54). In this work we aimed to characterize the Rox enzyme from *S. venezuelae*. Prior to this research, very little was known about Rox except that the sequence had high similarity to flavin-dependent monooxygenases. We cloned *rox* from *S. venezuelae* and expressed the enzyme heterologously in *E. coli*. We were able to crystalize Rox both in the presence and absence of RIF and solve the structure to using molecular replacement. The model for molecular replacement was a combination of the most similar proteins to Rox with their structures solved: PgaE, CabE, OxyS, and MtmOIV. These enzymes all have approximately 50% identity to Rox and consequently their structures are very similar (Appendix 2). PgaE and CabE are involved in angucycline biosynthesis, both catalyzing aromatic hydroxylase reactions. The structure of PgaE was solved by multiple wavelength anomalous diffraction (MAD), and the structure of CabE was solved by molecular replacement with PgaE as the search model (65). OxyS is an aromatic hydroxylase involved in oxytetracycline biosynthesis. MtmOIV is a Baeyer-Villiger monooxygenase, causing oxygen insertion and downstream non-enzymatic ring-opening. Both the OxyS and MtmOIV structures were solved by molecular replacement using PgaE as the search model (66,72). Despite these enzymes all being very similar in structure, they are divided by the reactions they catalyze: the aromatic hydroxylase and Baeyer-Villiger monooxygenase reactions. Both utilize a C(4a)-hydroperoxyflavin intermediate to transfer one oxygen from molecular oxygen to their substrates. The difference is that in the aromatic hydroxylase reaction, the C(4a)-hydroperoxyflavin acts as an electrophile, while in the Baeyer-Villiger reaction, the C(4a)-

hydroperoxyflavin is deprotonated and acts as a nucleophile, as illustrated in Figure 3.21 (63). Typical Baeyer-Villiger monooxygenases have sequence motifs that can be used to identify them from the protein sequence alone, and the structural fold is different than typical aromatic hydroxylases (67) (Appendix 2). However, MtmOIV is atypical; it looks like an aromatic hydroxylase from its sequence and structure, but has been shown to be a Baeyer-Villiger monooxygenase mechanistically (67). This makes it impossible to tell from the structure alone whether Rox is an aromatic hydroxylase or a Baeyer-Villiger monooxygenase.

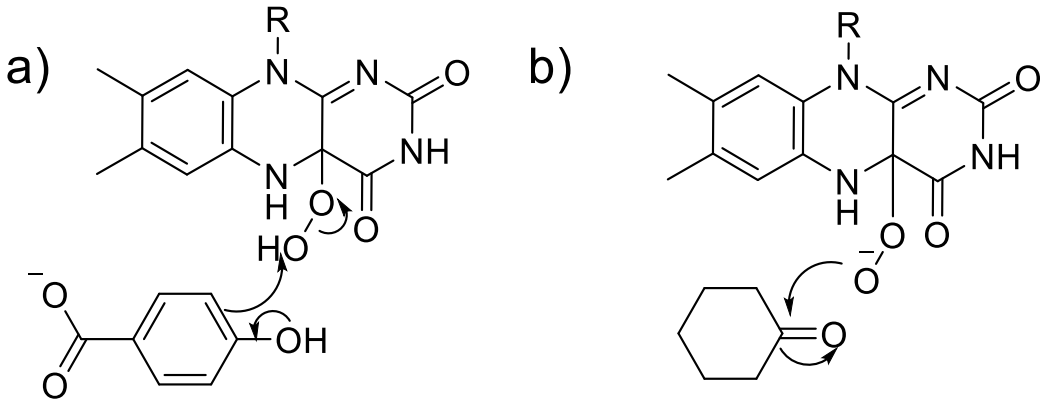

Figure 3.21 Comparing the aromatic hydroxylase and Baeyer-Villiger reactions. a) The aromatic hydroxylase reaction, in which the C(4a)-hydroperoxyflavin acts as an electrophile. b) The Baeyer-Villiger reaction, in which the C(4a)-hydroperoxyflavin anion acts as a nucleophile.

To confirm that Rox was capable of monooxygenating rifamycins as we expected from the sequence and structure of the enzyme, we set up an *in vitro* reaction. We were particularly interested in RIF-SV since this rifamycin does not have the C3 tail region that RIF does, which is where Rox was previously proposed to act. Two products were generated in the *in vitro* reaction; one 16 Da and one 18 Da larger than the starting material RIF-SV. We predicted the product mass would increase by the mass of one oxygen, which is consistent with the 16 Da increase. Rifamycins have a quinone-hydroquinone system at the C1 and C4 positions on the aromatic

core of the molecule (4). Mild reduction converts the quinone to the hydroquinone form, but ultimately the hydroquinone form will auto-oxidize to the quinone form in aerated, aqueous solution over time (73). This equilibrium causes both RIF-SV and RIF-S to be present in aqueous solution. This phenomenon might explain the second product of the *in vitro* reaction; it could be a hydroquinone form of the product RIF-SV-O. Nonetheless, we were encouraged to see the major product of 16 Da increase which we termed RIF-SV-O, and decided to move forward in characterizing this molecule. After purifying RIF-SV-O the structure was solved by NMR analysis performed by Dr. Kalinka Koteva, and is presented in Figure 3.18. Interestingly, the enzyme does act on the aromatic core, consistent with the high sequence and structural similarity to aromatic hydroxylases. The enzyme hydroxylates the C2 position, and the C2 nitrogen bond is broken in the RIF-SV-O structure. As determined in the SAR studies, the conformation of the ansa chain is essential for the activity of rifamycins, since it is this conformation that positions the 4 key hydroxyl groups correctly. By cleaving the ansa chain at C2, Rox completely alters the conformation of the RIF-SV molecule; it is logical to conclude that this is how the enzyme confers resistance to rifamycins. Indeed, RIF-SV-O demonstrated significantly reduced antibiotic activity in a disk diffusion activity in Figure 3.15 and in the MIC data in Table 3.2. Also of note from the RIF-SV-O structure is the C1/C4 quinone structure, as opposed to the hydroquinone scaffold in the starting material. This further supports the hypothesis that the second *in vitro* reaction product with a mass of 2 Da higher than RIF-SV-O could be a hydroquinone form of RIF-SV-O.

Based on mechanisms of structurally similar aromatic hydroxylases, we hypothesized that the source of the oxygen being incorporated into RIF-SV-O was molecular oxygen. To confirm this, we tested the reaction under anaerobic and labelled oxygen gas conditions. The

reaction did not occur in anaerobic conditions, and when the reaction was performed under an $^{18}O_2$ atmosphere the mass of the product increased by 2 Da, representing RIF-SV-^{18}O. This confirms that Rox uses molecular oxygen similar to other well characterized aromatic hydroxylases. We also observed that the enzyme showed no activity in the absence of a reducing co-substrate; this is also consistent with known mechanisms of aromatic hydroxylases.

The structural and mechanistic similarities to well characterized aromatic hydroxylases, and the structure of RIF-SV-O, led us to propose a mechanism for Rox. There are two parts to flavin dependant reactions: the reductive and reoxidative half reactions. The reductive half reaction is conserved among flavin dependant monooxygenases. A co-substrate, NAD(P)H in the case of aromatic hydroxylases, reduces the FAD flavin cofactor to $FADH_2$. The reduced flavin can then react with molecular oxygen to form C(4a)-hydroperoxyflavin. For aromatic hydroxylases, the reoxidative half reaction involves nucleophilic attack on the C(4a)-hydroperoxyflavin by the aromatic substrate, and we propose a similar mechanism for Rox. We propose that the C1 hydroxyl forms a C1 ketone group, and this allows for nucleophilic attack by C2 on the distal oxygen of the C(4a)-hydroperoxyflavin, as shown in Figure 3.15. This would form a rather unstable C2 hemiaminal intermediate. We propose that this leads to subsequent cleavage of the C2 nitrogen bond by ketone formation at C2. Finally, tautomerization of the di-ketone readily occurs, generating the final product RIF-SV-O. According to this mechanism, rifamycin substrates require a hydroxyl group at C1 for activation of the aromatic ring for nucleophilic attack. This could explain the limited affinity of the enzyme for rifabutin, a rifamycin with a ketone at C1. The very modest increase in MIC and HPLC product formation for rifabutin could be attributed to a tautomer of the molecule with a free hydroxyl at C1.

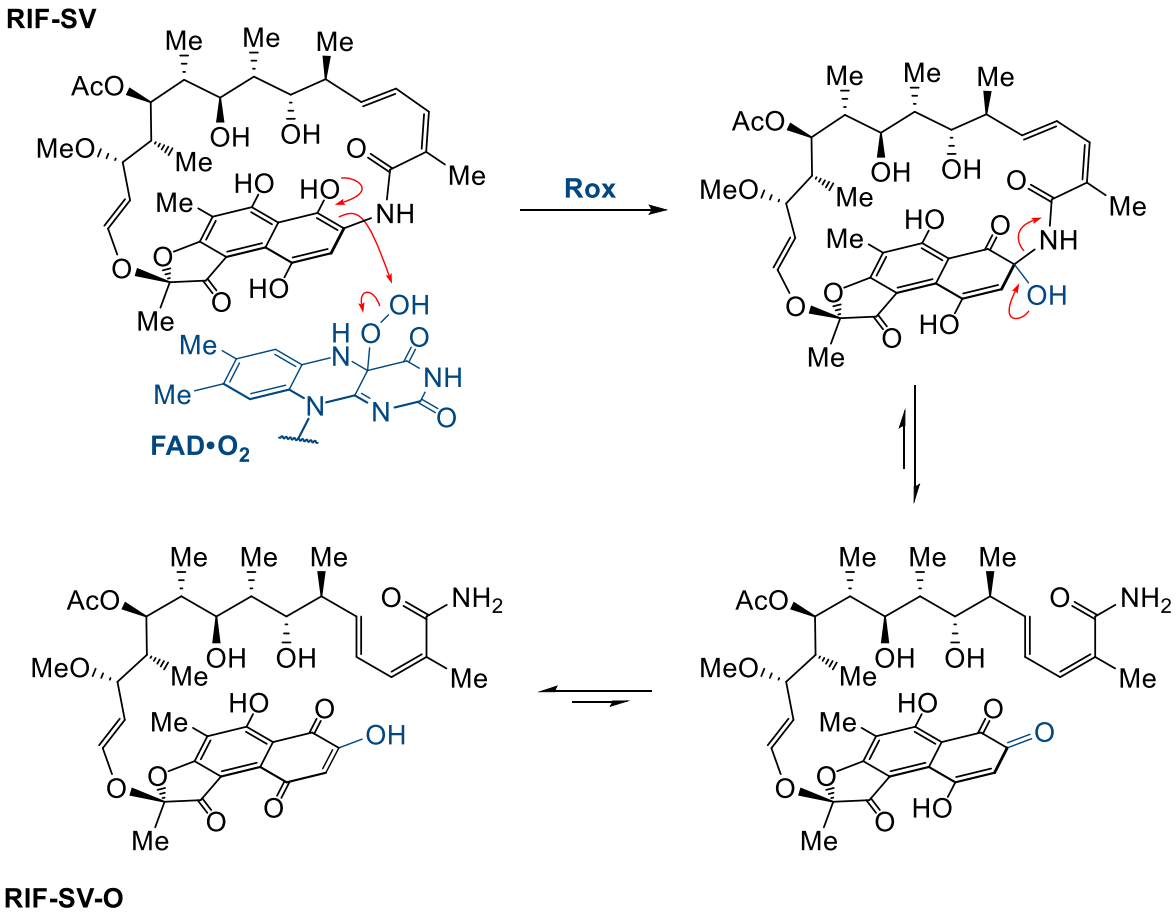

Figure 3.22 Proposed mechanism of Rox. The mechanism of the reductive half reaction is the same as that of pHBH, illustrated in Figure 3.2. NADH reduces the FAD to $FADH_2$, which recombines with molecular oxygen to form the C(4a)-hydroperoxyflavin (shown here in blue). The reoxidative half reaction is an electrophilic aromatic substation followed by a non-enzymatic rearrangement shown here.

In the canonical aromatic hydroxylase pHBH, a network of amino acids deprotonated the phenol to make the substrate a better nucleophile in the reoxidative half reaction. We looked at the active site of Rox for residues that may be involved in the deprotonation of the C1 hydroxyl group. The only candidate was His46; we proceeded to mutate this residue to a Gln. However, when the mutant Rox was assayed by HPLC it was found to have activity consistent with wild type Rox, indicating that His46 is not a necessary residue for catalysis. Further mutants can be

generated once the crystal structure of Rox is fully refined and we have a better idea of which residues may be involved.

We have proposed a mechanism for Rox that is consistent with the data generated in this thesis. This mechanism involves oxidative C-N bond cleavage by a monooxygenase, which to the best of our knowledge is the first example of this type of reaction. This is a new type of resistance to rifamycins, and the first example of monooxygenase mediated ring opening of an antibiotic conferring resistance. TetX has been shown to monooxygenate tetracycline conferring resistance, but this is caused by hemiketal formation within the molecule that leads to non-enzymatic polymerization of the molecule (69). TetX is not an aromatic hydroxylase; it acts on a β-diketone double bond instead of an aromatic ring. By cleaving the C2-N bond of the rifamycin scaffold, the conformation of the ansa chain is altered significantly, and this drastically reduces antibiotic activity. Cleavage of an antibiotic macrolactam ring causing resistance is precedented in a few cases. The enzyme Vgb cleaves the streptogramin B scaffold causing resistance by linearizing the antibiotic, and the Ere enzymes linearize macrolides by cleaving the macrolactam ring (77,78). However, these enzymes act by elimination and hydrolysis across an ester bond respectively.

We considered the Baeyer-Villiger type reaction for Rox. However, we discounted this type of mechanism for a few reasons. In the Baeyer-Villiger reaction, the C(4a)-hydroperoxyflavin acts as the nucleophile, attacking an electrophilic ketone carbon. RIF-SV does not have a suitable ketone on the aromatic core, but RIF-S has ketones at C1 and C4. However, we noted that rifamycins with a ketone at C1 were poor substrates for Rox, while other rifamycins with hydroxyl groups at C1 were better. As well, from the NMR analysis of RIF-SV-O, we are confident that C-N bond cleavage is occurring that gives rise to the two protons on the

nitrogen, and a Baeyer-Villiger type mechanism that resulted in this C-N bond cleavage could not be proposed that coincided with the available data. For these reasons, we do not believe that Rox is a Baeyer-Villiger type monooxygenase.

Chapter 4. Conclusions and future directions

4.1 Concluding remarks and future directions

In this work we examined the rifamycin resistome of *S. venezuelae*. Based on previous work from the Wright lab, we probed the genome for the presence of the RAE. We were specifically interested in *S. venezuelae* because this strain is widely used for *Streptomyces* genetics, and will be easily tractable for future research. We examined regions containing RAEs in *S. venezuelae,* along with the genes associated with the element. One of these genes, a rifampin monooxygenase *rox* conferred rifamycin resistance, while the putative helicase and glycosyltransferase did not. The promoter region upstream of *rox* responded to low levels of rifamycins to induce transcription, as was previously observed in WAC4747. The reporter strains of *S. venezuelae* generated in this work contain the *gusA* gene, which is a versatile reporter that can be used in many types of assays. These reporter strains will be useful in future studies involving the RAE. Pull down assays in *S. venezuelae* could be performed using the *rox* promoter region, in an attempt to identify an effector protein. Alternatively, RNA sequencing data could be obtained both in the presence and absence of low levels of RIF to observe genes that are upregulated, which may potentially inform on the process of induction by the RAE.

Once identified, the *rox* gene was cloned, overexpressed in *E. coli*, and biochemically characterized. We were able to crystallize Rox both in the presence and absence of the substrate RIF. The structure is very similar to other aromatic hydroxylases involved in natural product biosynthesis. RIF is bound mostly by hydrophobic residues adjacent to the FAD cofactor. We did not attempt to crystallize Rox with NADH bound; this could be done in the future to gain further insight into the enzyme mechanism.

We performed an in vitro reaction to determine whether Rox was capable of modifying rifamycins. Monooxygenated products could be observed for nearly all rifamycin substrates tested. We were intrigued to see that Rox monooxygenated RIF-SV, a rifamycin lacking a synthetic tail. We purified RIF-SV-O from a large scale in vitro reaction for structural analysis. The structure was solved by NMR and from this we concluded that the monooxygenation occurs on the aromatic core at C2, with a cleavage of the macrocyclic ring between the nitrogen and C2 occurring as well. This changes the conformation of the rifamycin scaffold, explaining both the decolourization and resistance mechanisms. From the structure of the enzyme and the product of the reaction, we propose a molecular mechanism for Rox similar to that of other aromatic hydroxylases, as seen in Figure 3.16. This monooxygenation mediated ring cleavage would be a new resistance mechanism and reaction type for a flavin dependant monooxygenase. The mechanism that we have proposed is from our work on RIF-SV; however, we speculate that this mechanism would be consistent with other rifamycins. This mechanism directly contradicts the presented structure of RIF-O by Hoshino and coworkers (55). Their procedure for obtaining RIF-O involved using resting cells overexpressing Rox. There is no way to be certain that RIF-O is a product of the enzyme; perhaps it is a by-product of some downstream reactions in the cell. Direct *in vitro* characterization of the Rox from *N. farcinica* would be useful and could perhaps be done in future to compare with Rox from *S. venezuelae*.

There remain a few questions about the Rox mediated decomposition process. Although we have proposed a mechanism by which Rox monooxygenates and inactivates rifamycins, further confirmation of the mechanism is needed. Detailed substrate binding studies would be useful in confirming the order of binding and reaction steps. The proposed reaction involves a number of intermediates post-enzymatic activity. Perhaps chemical trapping experiments could

be used to isolate these intermediates and further validate the mechanism. And although the proposed mechanism explains the inactivation and decolourization of rifamycins, it does not necessarily explain the decomposition. It remains unknown whether there are additional enzymes involved in the complete decomposition of rifamycins, or whether this is a non-enzymatic process. The extent to which the rifamycin scaffold is decomposed is unknown, since no fragments could ever be obtained. A thorough investigation of a rifamycin degradation using mass spectrometry analysis might be useful in elucidating this process.

Characterization of Rox presents a previously unknown inactivation mechanism of rifamycins. As we continue in an era of antibiotic resistance, we may find the rifamycins being repurposed for new treatment regimes. The rifamycin scaffold is also an attractive candidate for continued semi-synthesis. As these antibiotics experience a resurgence in popularity, the selective pressure for resistance is sure to increase. Understanding the rifamycin resistance determinants in the environment is sure to be an asset should they migrate to the clinic in the future.

References

1. Benveniste, R. & Davies, J. Aminoglycoside antibiotic-inactivating enzymes in actinomycetes similar to those present in clinical isolates of antibiotic-resistant bacteria. *Proc. Natl. Acad. Sci. U. S. A.* **70,** 2276–2280 (1973).

2. Wright, G. D. The antibiotic resistome: the nexus of chemical and genetic diversity. *Nat Rev Microbiol* **5,** 175–186 (2007).

3. Floss, H. G. & Yu, T. W. Rifamycin-mode of action, resistance, and biosynthesis. *Chem. Rev.* **105,** 621–632 (2005).

4. Sensi, P. History of the development of rifampin. *Clin. Infect. Dis.* **5,** 402–406 (1983).

5. Aristoff, P. A., Garcia, G. A., Kirchhoff, P. D. & Showalter, H. D. Rifamycins--obstacles and opportunities. *Tuberc.* **90,** 94–118 (2010).

6. Calvori, C., Frontali, L., Leoni, L. & Tecce, G. Effect of rifamycin on protein synthesis. *Nature* **207,** 417–418 (1965).

7. Hartmann, G., Behr, W., Beissner, K. A., Honikel, K. & Sippel, A. Antibiotics as inhibitors of nucleic acid and protein synthesis. *Angew. Chem. Int. Ed. Engl.* **7,** 693–701 (1968).

8. Wehrli, W., Knüsel, F., Schmid, K. & Staehelin, M. Interaction of rifamycin with bacterial RNA polymerase. *Proc. Natl. Acad. Sci. U.S.A.* **61,** 667–673 (1968).

9. McClure, W. R. & Cech, C. L. On the mechanism of rifampicin inhibition of RNA synthesis. *J. Biol. Chem.* **253,** 8949–8956 (1978).

10. Campbell, E. A. *et al.* Structural mechanism for rifampicin inhibition of bacterial RNA polymerase. *Cell* **104,** 901–912 (2001).

11. Gillespie, S. Evolution of drug resistance in *Mycobacterium tuberculosis*: clinical and molecular perspective. *Antimicrob. Agents Chemother.* **46,** 267–274 (2002).

12. David, H. L. Probability distribution of drug-resistant mutants in unselected populations of *Mycobacterium tuberculosis. Appl. Microbiol.* **20,** 810–814 (1970).

13. Ramaswamy, S. & Musser, J. M. Molecular genetic basis of antimicrobial agent resistance in *Mycobacterium tuberculosis:* 1998 update. *Tuber. Lung Dis.* **79,** 3–29 (1998).

14. Gagneux, S. *et al.* The competitive cost of antibiotic resistance in *Mycobacterium tuberculosis. Science* **312,** 1944–1946 (2006).

15. Mariam, D. H., Mengistu, Y., Hoffner, S. E. & Andersson, D. I. Effect of *rpoB* Mutations Conferring Rifampin Resistance on Fitness of *Mycobacterium tuberculosis*. *Antimicrob. Agents Chemother.* **48,** 1289–1294 (2004).

16. Reynolds, M. G. Compensatory evolution in rifampin-resistant *Escherichia coli*. *Genetics* **156,** 1471–1481 (2000).

17. Casali, N. *et al.* Evolution and transmission of drug-resistant tuberculosis in a Russian

population. *Nat. Genet.* **46,** 279–286 (2014).

18. Comas, I. *et al.* Whole-genome sequencing of rifampicin-resistant *Mycobacterium tuberculosis* strains identifies compensatory mutations in RNA polymerase genes. *Nat. Genet.* **44,** 106–110 (2012).

19. Hosaka, T. *et al.* Antibacterial discovery in actinomycetes strains with mutations in RNA polymerase or ribosomal protein S12. *Nat. Biotechnol.* **27,** 462–464 (2009).

20. Inaoka, T. & Ochi, K. Activation of dormant secondary metabolism neotrehalosadiamine synthesis by an RNA polymerase mutation in *Bacillus subtilis*. *Biosci. Biotechnol. Biochem.* **75,** 618–623 (2011).

21. Perkins, A. E. & Nicholson, W. L. Uncovering new metabolic capabilities of *Bacillus subtilis* using phenotype profiling of rifampin-resistant *rpoB* mutants. *J. Bacteriol.* **190,** 807–814 (2008).

22. Ochi, K., Tanaka, Y. & Tojo, S. Activating the expression of bacterial cryptic genes by *rpoB* mutations in RNA polymerase or by rare earth elements. *J. Ind. Microbiol. Biotechnol.* **41,** 403–414 (2014).

23. Vigliotta, G. *et al.* Natural merodiploidy involving duplicated *rpoB* alleles affects secondary metabolism in a producer actinomycete. *Mol. Microbiol.* **55,** 396–412 (2005).

24. Ishikawa, J., Chiba, K., Kurita, H. & Satoh, H. Contribution of *rpoB2* RNA polymerase β subunit gene to rifampin resistance in *Nocardia* species. *Antimicrob. Agents Chemother.* **50,** 1342–1346 (2006).

25. Hannula, M. & Hänninen, M.-L. Effect of putative efflux pump inhibitors and inducers on the antimicrobial susceptibility of *Campylobacter jejuni* and *Campylobacter coli*. *J. Med. Microbiol.* **57,** 851–855 (2008).

26. Hagman, K. E. *et al.* Resistance of *Neisseria gonorrhoeae* to antimicrobial hydrophobic agents is modulated by the mtrRCDE efflux system. *Microbiology* **141 (3),** 611–622 (1995).0

27. Okusu, H., Ma, D. & Nikaido, H. AcrAB efflux pump plays a major role in the antibiotic resistance phenotype of *Escherichia coli* multiple-antibiotic-resistance (Mar) mutants. *J. Bacteriol.* **178,** 306–308 (1996).

28. Maness, M. J. & Sparling, P. F. Multiple antibiotic resistance due to a single mutation in *Neisseria gonorrhoeae*. *J. Infect. Dis.* **128,** 321–330 (1973).

29. Louw, G. E. *et al.* A balancing act: efflux/influx in mycobacterial drug resistance. *Antimicrob Agents Chemother* **53,** 3181–3189 (2009).

30. Siddiqi, N. *et al. Mycobacterium tuberculosis* isolate with a distinct genomic identity overexpresses a tap-like efflux pump. *Infection* **32,** 109–111 (2004).

31. Gupta, A. K. *et al.* Microarray analysis of efflux pump genes in multidrug-resistant *Mycobacterium tuberculosis* during stress induced by common anti-tuberculous drugs. *Microb. Drug Resist.* **16,** 21–28 (2010).

32. Jiang, X. *et al.* Assessment of efflux pump gene expression in a clinical isolate *Mycobacterium tuberculosis* by real-time reverse transcription PCR. *Microb. Drug Resist.* **14,** 7–11 (2008).

33. Dabbs, E. R. Rifampicin inactivation by *Rhodococcus* and *Mycobacterium* species. *FEMS Microbiol. Lett.* **44,** 395–399 (1987).

34. Dabbs, E. R. *et al.* Ribosylation by Mycobacterial strains as a new mechanism of rifampin inactivation. *Antimicrob. Agents Chemother.* **39,** 1007–1009 (1995).

35. Morisaki, N. *et al.* Structure determination of ribosylated rifampicin and its derivative - new inactivated metabolites of rifampicin by Mycobacterial strains. *J. Antibiot. (Tokyo).* **48,** 1299–1303 (1995).

36. Quan, S. W., Venter, H. & Dabbs, E. R. Ribosylative inactivation of rifampin by *Mycobacterium smegmatis* is a principal contributor to its low susceptibility to this antibiotic. *Antimicrob. Agents Chemother.* **41,** 2456–2460 (1997).

37. Quan, S. *et al.* ADP-ribosylation as an intermediate step in inactivation of rifampin by a mycobacterial gene. *Antimicrob. Agents Chemother.* **43,** 181–184 (1999).

38. Tribuddharat, C. & Fennewald, M. Integron-mediated rifampin resistance in *Pseudomonas aeruginosa*. *Antimicrob. Agents Chemother.* **43,** 960–962 (1999).

39. Arlet, G. *et al.* Plasmid-mediated rifampin resistance encoded by an *arr-2*-like gene cassette in *Klebsiella pneumoniae* producing an ACC-1 class C β-lactamase. *Antimicrob. Agents Chemother.* **45,** 2971–2972 (2001).

40. Girlich, D. *et al.* Molecular epidemiology of the integron-located VEB-1 extended-spectrum β-lactamase in nosocomial enterobacterial isolates in Bangkok, Thailand. *J. Clin. Microbiol.* **39,** 175–182 (2001).

41. Da Fonseca, É. L., Freitas, F. D. S., De Amorim, J. C. & Vicente, A. C. P. Detection of new *arr*-4 and *arr*-5 gene cassettes in clinical *Pseudomonas aeruginosa* and *Klebsiella pneumoniae* strains from Brazil. *Antimicrob. Agents Chemother.* **52,** 1865–1867 (2008).

42. Houang, E. T. S., Chu, Y. W., Lo, W. S., Chu, K. Y. & Cheng, A. F. B. Epidemiology of rifampin ADP-ribosyltransferase (*arr*-2) and metallo-β-lactamase (*blaIMP-4*) gene cassettes in class 1 integrons in *Acinetobacter* strains isolated from blood cultures in 1997 to 2000. *Antimicrob. Agents Chemother.* **47,** 1382–1390 (2003).

43. Ueda, K. & Hayaishi, O. ADP-ribosylation. *Annu. Rev. Biochem.* **54,** 73–100 (1985).

44. Baysarowich, J. *et al.* Rifamycin antibiotic resistance by ADP-ribosylation: Structure and diversity of Arr. *Proc. Natl. Acad. Sci. U. S. A.* **105,** 4886–4891 (2008).

45. Yazawa, K. *et al.* Inactivation of rifampin by *Nocardia brasiliensis*. *Antimicrob. Agents Chemother.* **37,** 1313–1317 (1993).

46. Morisaki, N., Iwasaki, S., Yazawa, K., Mikami, Y. & Maeda, A. Inactivated products of rifampicin by pathogenic *Nocardia* spp.: structures of glycosylated and phosphorylated metabolites of rifampicin and 3-formylrifamycin SV. *J. Antibiot. (Tokyo).* **46,** 1605–1610

(1993).

47. Spanogiannopoulos, P., Thaker, M., Koteva, K., Waglechner, N. & Wright, G. D. Characterization of a rifampin-inactivating glycosyltransferase from a screen of environmental actinomycetes. *Antimicrob. Agents Chemother.* **56,** 5061–5069 (2012).

48. Tanaka, Y. *et al.* Different rifampicin inactivation mechanisms in *Nocardia* and related taxa. *Microbiol. Immunol.* **40,** 1–4 (1996).

49. Yazawa, K., Mikami, Y., Maeda, A., Morisaki, N. & Iwasaki, S. Phosphorylative inactivation of rifampicin by *Nocardia otitidiscavarium*. *J. Antimicrob. Chemother.* **33,** 1127–1135 (1994).

50. Dabbs, E. R. *et al.* Rifampicin inactivation by *Bacillus* species. *J. Antibiot. (Tokyo).* **48,** 815–819 (1995).

51. Spanogiannopoulos, P., Waglechner, N., Koteva, K. & Wright, G. D. A rifamycin inactivating phosphotransferase family shared by environmental and pathogenic bacteria. *Proc. Natl. Acad. Sci. U. S. A.* **111,** 7102–7107 (2014).

52. Stogios, P. J. *et al.* Rifampin phosphotransferase is an unusual antibiotic resistance kinase. *Nat. Commun.* **7,** 1-12 (2016).

53. Pocalyko, D. J., Carroll, L. J., Martin, B. M., Babbitt, P. C. & Dunaway-Mariano, D. Analysis of sequence homologies in plant and bacterial pyruvate phosphate dikinase, enzyme I of the bacterial phospoenolpyruvate:sugar phosphotransferase system and other PEP-utilizing enzymes. Identification of potential catalytic and regulatory motifs. *Biochemistry* **29,** 10757–10765 (1990).

54. Andersen, S. J., Quan, S., Gowan, B. & Dabbs, E. R. Monooxygenase-like sequence of a *Rhodococcus equi* gene conferring increased resistance to rifampin by inactivating this antibiotic. *Antimicrob. Agents Chemother.* **41,** 218–221 (1997).

55. Hoshino, Y. *et al.* Monooxygenation of rifampicin catalyzed by the rox gene product of *Nocardia farcinica*: structure elucidation, gene identification and role in drug resistance. *J. Antibiot. (Tokyo).* **63,** 23–28 (2010).

56. Roesch, L. *et al.* Pyrosequencing enumerates and contrasts soil microbial diversity. *ISME J.* **1,** 283–290 (2007).

57. Cuthbertson, L. & Nodwell, J. R. The TetR Family of Regulators. *Microbiol. Mol. Biol. Rev.* **77,** 440–475 (2013).

58. Schlimpert, S., Flärdh, K. & Buttner, M. Fluorescence Time-lapse Imaging of the Complete *S. venezuelae* Life Cycle Using a Microfluidic Device. *J. Vis. Exp.* e53863 (2016). doi:10.3791/53863

59. Spanogiannopoulos, P. Exploring Rifamycin Inactivation from the Soil Microbiome. (2014). at <https://macsphere.mcmaster.ca/handle/11375/16283>

60. Myronovskyi, M., Welle, E., Fedorenko, V. & Luzhetskyy, A. Beta-glucuronidase as a sensitive and versatile reporter in actinomycetes. *Appl. Env. Microbiol.* **77,** 5370–5383

(2011).

61. CLSI. M07-A10: Methods for Dilution Antimicrobial Susceptibility Tests for Bacteria That Grow Aerobically; Approved Standard—Tenth Edition. **35,** 1–87 (2015).

62. Kieser, T., Bibb, M. J., Buttner, M. J., Chater, K. F. & Hopwood, D. A. *Practical Streptomyces Genetics* (The John Innes Foundation, 2000)

63. Huijbers, M. M. E., Montersino, S., Westphal, A. H., Tischler, D. & Van Berkel, W. J. H. Flavin dependent monooxygenases. *Arch. Biochem. Biophys.* **544,** 2–17 (2014).

64. Entsch, B. & Van Berkel, W. J. Structure and mechanism of para-hydroxybenzoate hydroxylase. *FASEB J.* **9,** 476–483 (1995).

65. Koskiniemi, H. *et al.* Crystal structures of two aromatic hydroxylases involved in the early tailoring steps of angucycline biosynthesis. *J Mol Biol* **372,** 633–648 (2007).

66. Wang, P., Bashiri, G., Gao, X., Sawaya, M. R. & Tang, Y. Uncovering the enzymes that catalyze the final steps in oxytetracycline biosynthesis. *J. Am. Chem. Soc.* **135,** 7138–7141 (2013).

67. Bosserman, M. A., Downey, T., Noinaj, N., Buchanan, S. K. & Rohr, J. Molecular insight into substrate recognition and catalysis of Baeyer-Villiger monooxygenase MtmOIV, the key frame-modifying enzyme in the biosynthesis of anticancer agent mithramycin. *ACS Chem Biol* **8,** 2466–2477 (2013).

68. Hiromoto, T., Fujiwara, S., Hosokawa, K. & Yamaguchi, H. Crystal structure of 3-hydroxybenzoate hydroxylase from *Comamonas testosteroni* has a large tunnel for substrate and oxygen access to the active Site. *J. Mol. Biol.* **364,** 878–896 (2006).

69. Yang, W. *et al.* TetX is a flavin-dependent monooxygenase conferring resistance to tetracycline antibiotics. *J Biol Chem* **279,** 52346–52352 (2004).

70. Roy, A., Kucukural, A. & Zhang, Y. I-TASSER: a unified platform for automated protein structure and function prediction. *Nat Protoc* **5,** 725–738 (2010).

71. Kallio, P. *et al.* Flavoprotein hydroxylase PgaE catalyzes two consecutive oxygen-dependent tailoring reactions in angucycline biosynthesis. *Biochemistry* **50,** 5535–5543 (2011).

72. Beam, M. P., Bosserman, M. A., Noinaj, N., Wehenkel, M. & Rohr, J. Crystal Structure of Baeyer− Villiger Monooxygenase MtmOIV, the Key Enzyme of the Mithramycin Biosynthetic Pathway. *Biochemistry* **48,** 4476–4487 (2009).

73. Sensi, P., Timbal, M. T. & Maffh, G. Rifomycin IX two new antibiotics of rifomycin family: Rifomycin S and rifomycin SV - Preliminary report. *Experientia* **16,** 412 (1960).

74. Hewavitharana, A. K., Shaw, P. N., Kim, T. K. & Fuerst, J. A. Screening of rifamycin producing marine sponge bacteria by LC-MS-MS. *J. Chromatogr. B. Anal. Technol. Biomed. Life Sci.* **852,** 362–366 (2007).

75. Kim, T. K., Hewavitharana, A. K., Shaw, P. N. & Fuerst, J. A. Discovery of a new source of rifamycin antibiotics in marine sponge actinobacteria by phylogenetic prediction. *Appl.*

Env. Microbiol. **72,** 2118–2125 (2006).

76. D'Costa, V. M., McGrann, K. M., Hughes, D. W. & Wright, G. D. Sampling the antibiotic resistome. *Science* **311,** 374–377 (2006).

77. Mukhtar, T. A., Koteva, K. P., Hughes, D. W. & Wright, G. D. Vgb from *Staphylococcus aureus* inactivates streptogramin B antibiotics by an elimination mechanism not hydrolysis. *Biochemistry* **40,** 8877–8886 (2001).

78. Morar, M., Pengelly, K., Koteva, K. & Wright, G. D. Mechanism and diversity of the erythromycin esterase family of enzymes. *Biochemistry* **51,** 1740–1751 (2012).

Appendices

Appendix 1. List of primers used

Primer name	Direction	Sequence	Purpose
Prgt-F	Forward	5'-atgcattctagacggccccggaggcgcg-3'	Cloning Prgt into pGUS plasmid
Prgt-R	Reverse	5'-atgcatggtacccggctcgacgctcccgcg-3'	
Prox-F	Forward	5'-atgcattctagacgctacctcagcccccggc-3'	Cloning Prox into pGUS plasmid
Prox-R	Reverse	5'-atgcatggtaccgagaaccgccccgtttccgc-3'	
Phel-F	Forward	5'-atgcattctagaggacggccgggtacggg-3'	Cloning Phel into pGUS plasmid
Phel-R	Reverse	5'-atgcatggtaccgaggtgagtctcatttctgcaggtcctg-3'	
Rox_F	Forward	5'-atgcatcatatgatgtttgacgtgatcgttgtcgg-3'	Cloning *rox* into pET28a
Rox_R	Reverse	5'-atgcatggatcctcagccggccgtggc-3'	
Rgt_F	Forward	5'-atgcatcatatgatggtggggctcgccgtg-3'	Cloning potential *rgt* into pET28a
Rgt_R	Reverse	5'-atgcatggatccctaccgcgtcgcggcgc-3'	
Hel_F	Forward	5'-atgcatcatatggtgcgtgtgctttcgtc-3'	Cloning putative helicase into pET28a
Hel_R	Reverse	5'-atgcatggatcctcaggagctggtgaggatc-3'	
c138g_F	Forward	5'-gcaggggctgcaggtccgcagcatc-3'	Site directed mutagenesis of *rox*
c138g_R	Reverse	5'-atcacctcgatgctgcggacctgcagc-3'	

Appendix 2. Structures of monooxygenases used to generate Rox model

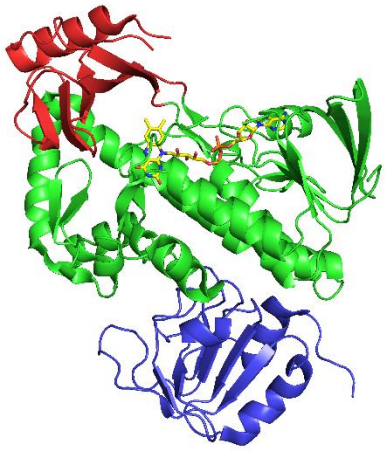

PgaE

PDB: 2QA1

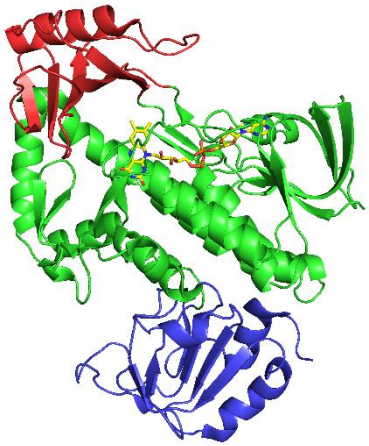

CabE

PDB: 2QA2

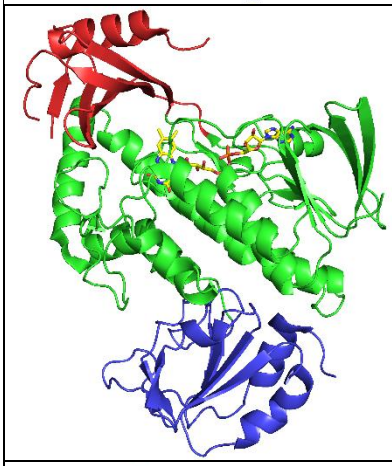

OxyS

PDB: 4K2X

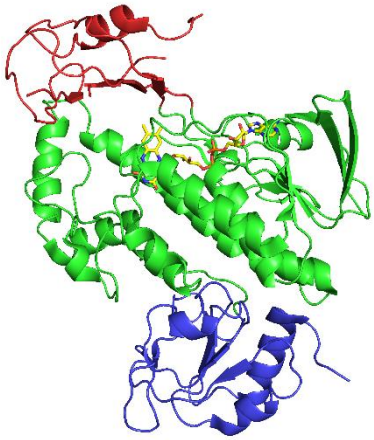

MtmOIV

PDB: 3FMW

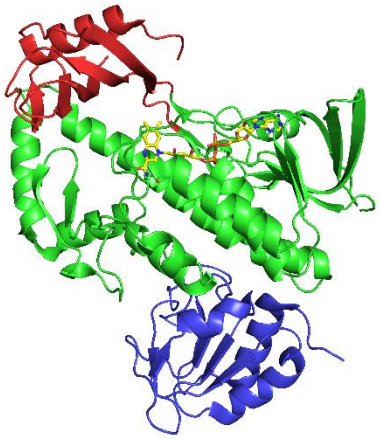

MtmOIV

PDB: 4K5S

Appendix 3. ^{1}H and ^{13}C chemical shifts of RIF-SV-O

#	^{1}H	^{13}C
1		181.56
2		132.18
3	6.10 (s, 1H)	111.44
4		185.96
5		105.39
6		171.55
7		113.21
8		165.88
9		109.22
10		127.48
11		190.4
12		111.56
13	1.65 (s, 3H)	20.12
14	2.14 (s, 3H)	7.32
15		170.52
16		130.45
17	6.01 (d, 1H)	131.46
18	6.54 (dtd, 1H)	126.4
19	5.75 (dd, 1H)	140.67
20	2.19 (q, 1H)	40.32
21	3.54 – 3.44 (m, 1H)	74.92
22	1.75 (m, 1H)	33.97
23	3.07 (dd, 1H)	75.93
24	1.57 (ddt, 1H)	39.75
25	5.24 (d, 1H)	72.53
26	1.75 (m, 1H)	36.57
27	3.54 – 3.44 (m, 1H)	73.45
28	5.18 – 5.09 (m, 1H)	112.13
29	6.33 (d, 1H)	141.33
30	1.94 (s, 3H)	20.85
31	0.85 (d, 3H) **	16.43
32	0.85 (d, 3H) **	10.92
33	0.72 (d, 3H)	9.83
34	0.69 (d, 3H)	10.14
35		169.74
36	1.94 (s, 3H)	21.02
37	2.91 (s, 3H)	55.17
NH	7.06 (s, 1H)	
	7.24 (d, 1H)	
OH		
OH	4.59-OH (21)	
OH	4.43-OH (23)	

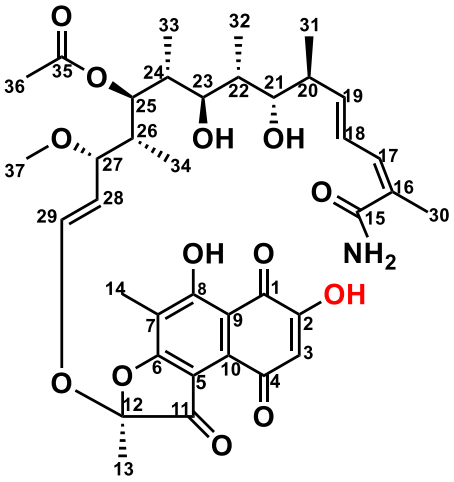

Appendix 4. ^{1}H and ^{13}C chemical shifts of RIF-S

#	^{1}H	^{13}C
1		181.78
2		140.11
3	7.31 (s, 1H)	118.55
4		184.78
5		107.06
6		171.87
7		114.36
8		165.89
9		110.14
10		130.55
11		191.23
12		111.17
13	1.65 (s, 3H)	21.48
14	2.20 (s, 3H)	7.5
15		170.29
16		130.1
17	6.20 (d, 1H)	131.63
18	6.07 (dd, 1H)	124.46
19	5.81 (dd, 1H)	141.35
20	1.45 (m, 1H)	39.12
21	3.51 (dd, 1H)	72.22
22	1.61 (q, 1H)	32.71
23	2.90 (d, 1H)	75.97
24	1.45 (m, 1H)	36.83
25	5.10 – 5.02 (m, 1H)	72.22
26	2.06 (h, 1H)	39.82
27	3.26 (dd, 1H)	77.89
28	5.10 – 5.02 (m, 1H)	116.66
29	6.14 (d, 1H)	142.87
30	1.98 (s, 3H)	19.87
31	0.79 (d, 3H)	17.32
32	0.84 (d, 3H)	11.67
33	0.57 (d, 3H)	9.41
34	0.17 (d, 3H)	10.08
35		169.82
36	1.93 (s, 3H)	20.85
37	2.98 (s, 3H)	55.66
NH	9.71	
OH	12.66	
OH	4.38	
OH	4.35	

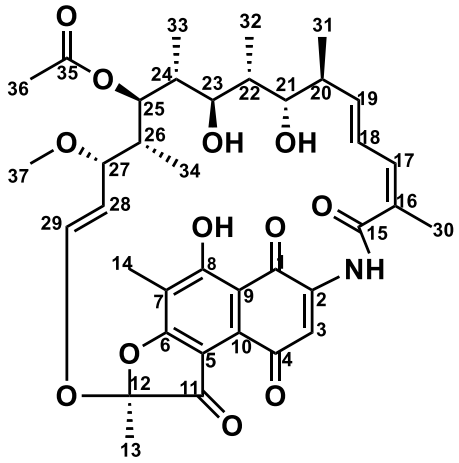

Appendix 5. ^{1}H and ^{13}C chemical shifts of RIF-SV

#	^{1}H	^{13}C
1		145.17
2		119.37
3	7.12 (s, 1H)	111.59
4		145.34
5		114.07
6		171.96
7		100.26
8		114.07
9		115.88
10		98.72
11		184.53
12		108.73
13	1.60 (s, 3H)	22.35
14	1.89 (s, 3H)	7.47
15		168.07
16		133.35
17	6.09 (d, 1H)	129.87
18	6.38 (dd, 10.8 Hz, 1H)	125.48
19	5.96 (dd, 1H)	138.52
20	2.17 (q, 1H	38.44
21	3.72 (s, 1H)	72.83
22	1.65 (d, 1H)	33.27
23	2.88 – 2.82 (m, 1H)	76.05
24	1.32 (d, 1H)	38.11
25	5.05 (d, 1H	73.57
26	1.08 (d, 1H)	40.54
27	3.24 (dd, 1H)	76.63
28	4.93 (dd, 1H)	117.43
29	6.24 (d, 1H)	143.22
30	1.92 (s, 3H)	20.03
31	0.84 (d, 3H)	18.49
32	0.88 (d, 3H)	11.77
33	0.53 (d, 3H)	8.61
34	0.53 (d, 3H)	9.03
35		169.91
36	1.99 (s, 3H)	20.81
37	2.89 (s, 3H)	55.76
NH	8.55 (s, 1H)	
OH	11.60 (s, 1H)	
OH	4.23 (d, 1H)	
OH	4.67 (s, 1H)